A fast simulation tool for ship grounding damage analysis

Jean-Philippe Pineau, Fabien Conti, Hervé Le Sourne, Thibaut Looten

Version of Record: https://www.sciencedirect.com/science/article/pii/S0029801822015475
Manuscript_6b7e61d53683725ba8cfd093635834fb

A fast simulation tool for ship grounding damage analysis

Jean-Philippe Pineau [a,b], Fabien Conti [c], Hervé Le Sourne [a,b] , Thibaut Looten [b]
[a] Nantes Université, Ecole Centrale Nantes, CNRS UMR 6183 - Nantes, France
[b] ICAM Engineering School - Nantes, France
[c] Bureau Veritas, Marine and Offshore - Nantes, France

Abstract— This paper presents a numerical tool based on analytical formulations for rapid assessment of damage in ship grounding accidents. Through a step-by-step solution, the ship resistant force is assessed by the super-element method and transferred to a 6-DoF external dynamics solver, which updates the global ship motion by taking into account the action of hydrodynamic forces. The two-way coupled solver is first confronted to finite element simulations considering a 34-kTons cruise ship in bottom and side grounding situations. It is then used to simulate thousands of scenarios, varying the rock shape, the ship impact location, initial penetration and velocity as well as rock/hull friction coefficient. In this way, the influence of ship structural properties (shell thickness, material grade, etc.) on the breach size is investigated. The highest breach reductions are obtained by increasing either the outer shell thickness or the material grade, while acting on transverse frames marginally affects the damage extent. It also appears that a bottom impact is systematically more damaging than a side impact, all else being equal. Likewise, a structural reinforcement is demonstrated to be more efficient in bottom grounding than in side grounding. This is because in side grounding situation, the ship is pushed away by rock and thus undergoes significant sway, yaw and sometimes roll motions that limit the damage extent. Finally, friction is shown to be of primary importance in bottom grounding, while its effect is rather limited in side grounding.

Keywords: *Ship grounding, Super-element, Finite element, Ship crashworthiness, Fluid-structure interaction, Coupled simulation*

1 Introduction

Recent accidents of the MV Wakashio and Costa Concordia have shown that although the maritime sector is continually investing in increasing and maintaining safety on board ships, further efforts are needed to limit the number and consequences of ship accidents. Currently, to minimise the damage extent and hence the probability of capsize during and after a ship collision or ship grounding event, the maritime sector refers to the SOLAS2009 and SOLAS2020 regulatory instruments [1]. SOLAS2020 regulation is based on probabilistic damage distributions derived from statistic analyses of real ship accidents (mainly cargo ships). In addition, SOLAS requirement does not depend on the ship scantlings (presence of a double hull for instance) or on the energy absorption capacity (material, plating thickness...) since the damage distribution is only driven by ship length, width and draft. Consequently, when a new ship is designed, it can be very difficult to quantify the effect of the new design on collision/grounding damage reduction.
To analyse the crashworthiness of grounded ships, scaled experiments have been conducted in the 90's by *Rodd & Sikora* [2] and *Turgeon* [3] and more recently by *Calle et al.* [4] and *Chen et al.* [5]. However, such experiments remain very expensive and of course hard to perform on full scale vessels. Nowadays, nonlinear finite element analysis (NLFEA) appears to be a good alternative for assessing the damage suffered by a ship involved in a grounding event and many research works have been reported on this topic [6–10]. Nonetheless, despite the increasing capacity of computers, the use of high fidelity models is not always possible as both the model set-up and numerical solution may be very time consuming. To have an idea, the numerical simulation of a $130m$-long ship bottom raking over a sharp rock may last more than 10 days using a parallel 12 CPUs Intel core i7 computer. As a consequence, NLFEA is not well suited at pre-design stage or when a full grounding risk analysis involving many ship velocities, rock shapes and impact locations is needed.
As an alternative, simplified analytical solutions have been derived for the primary components of a ship hull namely outer/inner hull, longitudinal girders and transverse floors. The response of bottom plating was particularly investigated by *Simonsen* [11], *Wang et al.* [12], *Zeng et al.* [13], *Heinvee* [10] for the so-called

raking scenarios in which the outer shell is perforated and by *Turgeon* [3] and *Hong & Amdahl* [14] for the *sliding* scenarios in which the structure is indented without rupture. Sliding and raking responses of transverse floors have also been studied by many authors [11, 12, 14–18] while less research work has been carried out on longitudinal girders [11, 18–20].
According to *Alsos & Amdahl* [21], both the shape and the size of the rock greatly influence the ship damage. Closed-form expressions reported in aforementioned papers have been derived considering wedge and conical shaped rocks for ship raking scenarios and truncated pyramids for sliding grounding events. A unique rock idealisation suitable for both sliding and raking problems was later proposed by *Nguyen et al.* [22] and *Heinvee & Tabri* [23], who modelled the rock as an elliptic paraboloid and performed finite element simulations. Such a shape allows to represent both sharp and shallow rocks by varying only the two parameters C and E of the following parabolic equation:

$$z_r = -Cx_r^2 - Ey_r^2 \tag{1}$$

Where x_r, y_r and z_r denote the coordinates of a point located on the paraboloid and C and E are the rock curvatures along longitudinal and transverse direction respectively.
Very recently, the authors of the present paper derived analytical formulas based on plastic limit analysis to assess the resistance of a ship bottom raking [17] and sliding [18] on a paraboloid shaped rock.
It is also noteworthy that as recently highlighted by *Bulian et al.* [24, 25], very few researches have been conducted on side grounding. Moreover, regarding ship grounding analyses, except in the recent work of *Taimuri et al.* [26], the action of the surrounding water is either completely ignored or accounted for very simply through the use of an added mass coefficient - see for instance [9, 27, 28].

In this context and as a continuation of the work reported by the authors in [17] and [18], this paper presents the resulting simplified structural solver named *FLAGS* (**FL**ARE **G**rounding **S**olver), which has been developed in the framework of EU-project FLARE[1]. The program is based on the Super-Element approach and is coupled with the existing external dynamics program *MCOL* [29] to account for the action of the surrounding water. The main advantage of the resulting tool is that thousands of grounding scenarios can be analysed in a relatively short time, which renders such approach very efficient for ship damage stability analyses as well as crashworthiness optimisation.

The objectives of the present paper are thus: (i) to describe in Section 2 the functioning of *FLAGS/MCOL*, (ii) to explain in Section 3 how this tool has been validated for both ship bottom and ship side grounding analyses, (iii) to present in Section 4 the structural sensitivity analyses that have been performed on a given cruise ship thanks to the rapidity of the coupled solvers.

2 Method

The objective of this section is to present the simplified program *FLAGS/MCOL*, i.e. its global functioning and the different modules, while its graphical user interface (GUI) is presented in Appendix A. Both *FLAGS* solver and its graphical interface were developed in Java language.

Ship collision or grounding analysis is commonly split into two distinct processes:

- External dynamics
- Internal mechanics

On one hand, *external dynamics* target the global rigid body movements of the ship, which are governed not only by the impact force but also by the hydrodynamic loads acting on the immersed part of the hull. *Internal mechanics*, on the other hand, focuses on the modes of deformation and failure of the crushed components: bottom/double bottom, floors and girders in bottom grounding ; hull plating, decks and bulkheads in side grounding. Recently, *Le Sourne et al.* [30] demonstrated that deformation mechanisms and ship overall motions may be strongly coupled in ship grounding. Indeed, the force exerted by the rock may push vertically and/or transversely the ship and, depending on the position of the rock with respect to the ship centre of gravity, modify its roll, yaw and pitch angles. In return, buoyancy forces may affect significantly the ship kinematics and consequently the damage distribution. Finally, a ship running aground over a sharp rock may result in flooding of the breached compartments. Water ingress modifies the mass of the ship and consequently its stability as

[1] **FL**ooding **A**ccident **RE**sponse: `https://www.flare-project.eu/`

both the draft and roll and/or pitch angles will change. In return, these changes will affect the deformation modes and damaged areas.

In this study, the effect of water ingress throughout the grounding event on the ship hydrodynamic response is neglected. External dynamics are treated following a *semi-coupled* approach via the use of *MCOL* solver, while internal mechanics are modelled through the Super-Element method implemented in *FLAGS* solver.

As depicted in Figure 1, the resulting tool is composed of three modules: the first one detects the impacted structural components (the so-called super-elements), the second calculates each S.E. resisting force and the third module updates the ship rigid-body movement by taking into account the action of hydrodynamic forces. These three modules as well as the procedures to calculate the time step and to stop the iterative process are now briefly presented.

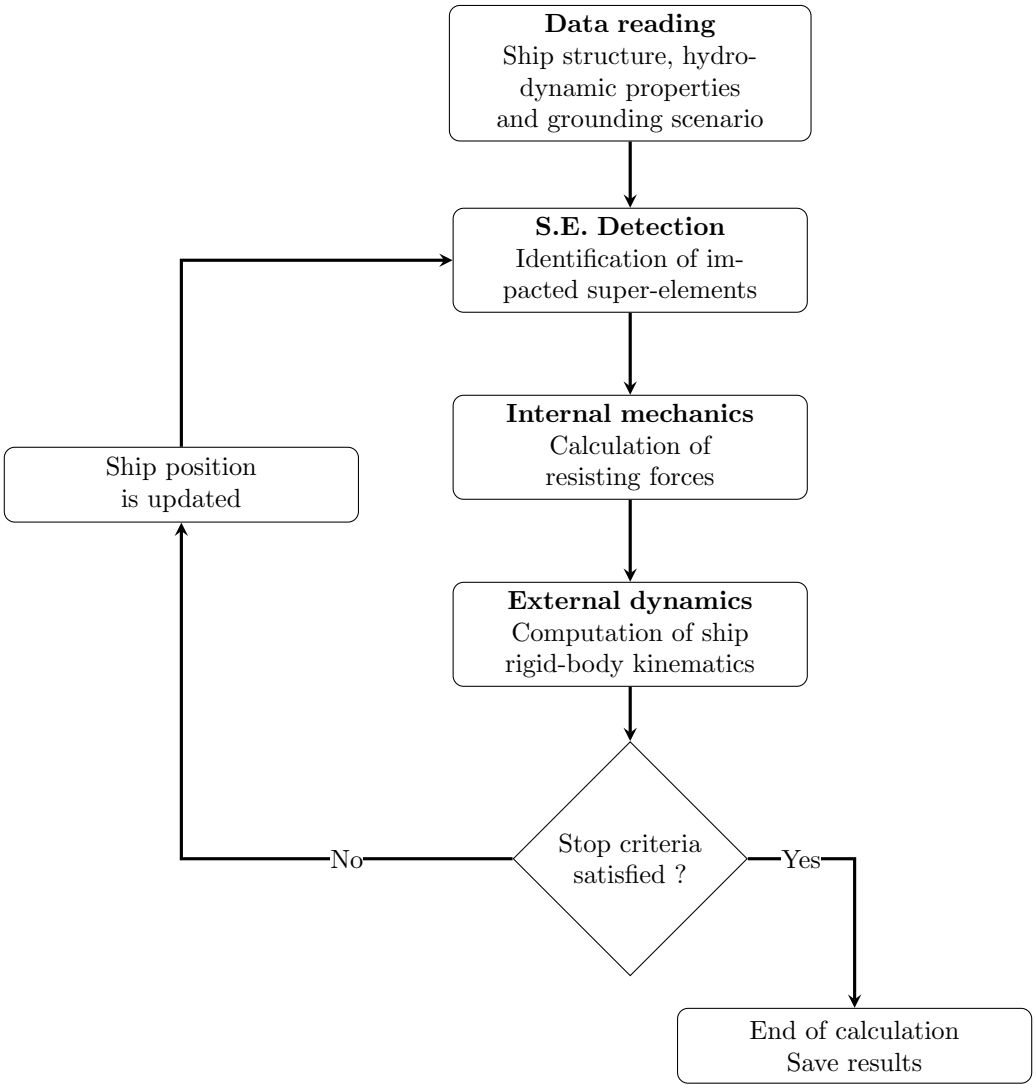

Figure 1: Flowchart of *FLAGS/MCOL* program

2.1 Super-elements detection

First and foremost, at beginning of each time step, the different Super-Elements that have been impacted by the rock must be detected. One possibility to obtain the list of the impacted elements might be to apply a detection algorithm to the entire ship structure. Nevertheless, since the bottom hull may contain hundreds of S.E, doing so would reduce the effectiveness in term of computation time. Therefore, the Super-Elements located in the circle of radius R_d and centred at the rock apex R are first identified. They are highlighted in orange on Figure 2. An impact detection algorithm is then applied to the surrounding elements and various quantities such as the rock vertical penetration (H) into the element are calculated.

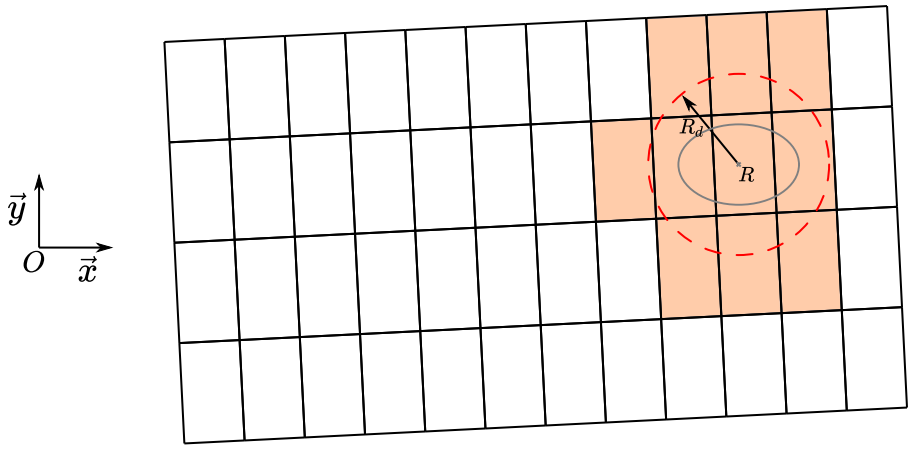

Figure 2: Pre-filter detection procedure

In the following, the equations are written for the case of an outer/inner bottom plating. Note however that the procedure has also been adapted to the floors, girders, floor/girder intersections, side shell, bulkheads, decks and deck/bulkhead intersections.

In the earth-fixed coordinate system, the equation of the rock writes:

$$z = Z_0 - C(x - X_0)^2 - E(y - Y_0)^2 \tag{2}$$

Where X_0, Y_0 and Z_0 are the initial coordinates of the rock apex provided as input data. All the flat plate elements may be described by the following Cartesian equation:

$$ax + by + d + z = 0 \tag{3}$$

Where a, b and d are three coefficients depending on the connecting node coordinates (X, Y, Z). From Eqs. 2 and 3, the intersection of a Super-Element with the rock can be summarised by the following quadratic form:

$$K_1 x^2 + K_2 xy + K_3 y^2 + K_4 x + K_5 y + K_6 = 0 \tag{4}$$

Where $K_{i\ 1 \leq i \leq 6}$ are expressed as:

$$\begin{cases} K_1 = C \\ K_2 = 0 \\ K_3 = E \\ K_4 = -a - 2CX_0 \\ K_5 = -b - 2EY_0 \\ K_6 = CX_0^2 + EY_0^2 - d - Z_0 \end{cases} \tag{5}$$

Equation 4 may be rewritten in matrix form as:

$$\begin{pmatrix} x & y \end{pmatrix} \begin{pmatrix} K_1 & K_2 \\ K_2 & K_3 \end{pmatrix} \begin{pmatrix} x \\ y \end{pmatrix} + \begin{pmatrix} K_4 & 0 \\ 0 & K_5 \end{pmatrix} \begin{pmatrix} x \\ y \end{pmatrix} + K_6 = 0 \tag{6}$$

With a paraboloid rock shape, $K_2 = 0$ so Eq. 4 simply writes:

$$K_1 (x')^2 + K_3 (y')^2 + K_7 = 0 \tag{7}$$

With :

$$\begin{cases} x' = x - \frac{1}{2} K_4 / K_1 \\ y' = y - \frac{1}{2} K_5 / K_3 \\ K_7 = K_6 - \frac{1}{K_1} \left(\frac{K_4}{2} \right)^2 - \frac{1}{K_3} \left(\frac{K_5}{2} \right)^2 \end{cases} \tag{8}$$

Finally, depending on the sign of K_7, one obtain:

$$\begin{cases} K_7 = 0 & \textit{Intersection is reduced to a point} \\ K_7 < 0 & \textit{Intersection is reduced to an ellipse} \\ K_7 > 0 & \textit{No intersection} \end{cases} \tag{9}$$

Since a Super-Element is a finite plane surface, a simple procedure is applied to check if the rock is actually inside the Super-Element when the intersection reduces to an ellipse or a point. Then, the centre of the ellipse as well the penetration into the S.E are calculated.

2.2 Time step computation

Defining the time step requires to find a compromise between a small value that provides accurate results at the cost of an important computation effort, and a large one that allows for rapid computation but with lower accuracy.

For ship grounding application, the time step Δt should be small enough to ensure that no transverse structure will be missed between two successive iterations. In addition, since the dissipated energy is calculated as the integral of the force-displacement curve, the time step should be small enough to integrate with sufficient accuracy. Based on several analyses, the time step has been set to:

$$\Delta t = \frac{R_x}{V_x}\frac{1}{10} \tag{10}$$

Where R_x and V_x are respectively the longitudinal radius of the rock into the outer shell and the ship surge velocity. Equation 10 ensures that 10 iterations are performed during the crushing of a transverse floor, which appears sufficient to accurately capture the evolution of the resisting forces. Besides, as the ship slows down, the surge velocity V_x decreases and consequently the time step interval Δt should be allowed to increase. Then, for sake of efficiency, the time step is reevaluated every 100 iterations based on the actual surge velocity $V_x(t)$. Figure 3 illustrates a typical evolution of the time step Δt with the number of iteration. It should be emphasised that the user can also define a constant time step in the *Scenario.xml* file.

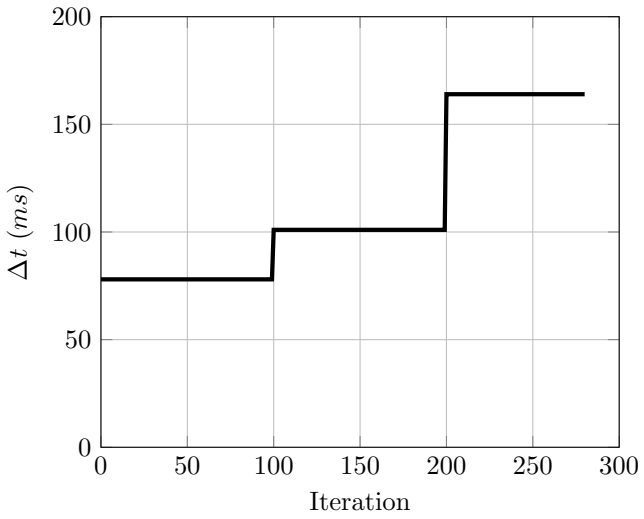

Figure 3: Typical evolution of time step interval

2.3 Stop criteria

The calculation procedure continues until one of the following stop criteria is satisfied:

1. $V_x = 0$
2. Out of ship

The first condition corresponds to the case where the entire ship initial kinetic energy has been dissipated through plastic deformation and friction. At the end of the calculation, the ship is at rest. The second condition corresponds to a ship that has been entirely damaged (along its full length), or has "escaped" from the rock (after a heave, roll or sway movement for instance). The ship final kinetic energy is not necessarily zero but the calculation stops as soon as the ship is no longer in contact with the rock.

2.4 Internal mechanics

The Super-Element method, initially introduced by *Lützen* [31] for ship collision analysis, consists in splitting the structure into an assembly of large and independent substructures, the so-called Super-Elements (S.E). For each of them, closed-form solutions are derived to evaluate their resisting force and the energy they dissipate by plastic deformation and friction. A reduced number of S.E. as well as analytical solutions make this approach very efficient for simulating ship collision or grounding events [32, 33]. Specifically, closed-form solutions are found using the Upper bound theorem of plasticity [34], which states that the force causing the collapse of a given structure may be found by equating the power of external loads to the rate of energy dissipated by plastic deformation and friction. In ship grounding analysis, such equilibrium may be expressed as:

$$F_L V_x + F_T V_y + F_V V_z = \dot{E}_i + \int_S \mu p V_{rel}\, dS \tag{11}$$

Where :
F_L : longitudinal resisting force
F_T : transverse resisting force
F_V : vertical resisting force
V_x : ship surge velocity
V_y : ship sway velocity
V_z : heave velocity
$\dot{E}_i$: internal energy rate
μ : friction coefficient between ship and rock
p : normal pressure of the rock from element dS
V_{rel}: relative velocity between ship and rock
S : contact area between rock and plate

The problem thus comes to find an analytical expression of the internal energy rate and this is commonly done under the following assumptions:

1. The structural elastic deformation is neglected. According to *Pedersen & Li* [35], the energy absorbed elastically only represents less than 6% of the overall impact energy.
2. Considering the ship velocity at instant of impact and according to *Jones* [34] or *Çerik & Choung* [6], structural dynamic effects like inertial forces and strain rate effect are disregarded.
3. The material is assumed to be rigid-perfectly plastic so its behaviour law is defined by a unique flow stress σ_0.
4. Finally, membrane and bending deformations are assumed to be decoupled.

Let us take for instance the case of a plate subject to out-of-plane loading. Under above hypotheses, the rate of energy absorbed by plastic deformation is the sum of bending energy rate ($\dot{E}_b$) and membrane ($\dot{E}_m$) energy rate expressed as:

$$\dot{E}_b = \int_S M_{\alpha\beta}\dot{k}_{\alpha\beta}\, dS + \sum_{i=1}^{n} M_{0i}\dot{\theta}_i l_i \tag{12}$$

$$\dot{E}_m = \frac{2}{\sqrt{3}}\sigma_0 t_h \int_S \sqrt{\dot{\varepsilon}_x^2 + \dot{\varepsilon}_y^2 + \dot{\varepsilon}_{xy}^2 + \dot{\varepsilon}_x\dot{\varepsilon}_y}\, dS \tag{13}$$

Where $N_{\alpha\beta}$ and $M_{\alpha\beta}$ are the membrane force and bending moment, $\dot{\varepsilon}_{\alpha\beta}$ and $\dot{k}_{\alpha\beta}$ are the generalised strain and curvature rates, and $\dot{\theta}_i$ and l_i are the rotation rate and length of the i^{th} plastic hinge line.

In fact, the main difficulty lies in postulating a realistic displacement field for each S.E. and in finding its main mechanisms of deformation. Analytical expressions that have been derived and implemented in *FLAGS* solver are detailed in *Pineau et al.* [17] for ship raking and in *Pineau et al.* [18] for ship sliding. It should also be emphasised that small secondary stiffeners are not considered explicitly but smeared into the thickness of the supporting panels - see [36–40] for instance.

2.5 External dynamics

Initially developed at the end of the 90's by Mitsubishi Heavy Industry, the external dynamics program *MCOL* was completely rewritten by *Le Sourne et al.* [29] who included large rotational movements as well as Coriolis and drag damping forces for ship-submarine collision analysis. Resulting solver was then implemented in *Ls-Dyna* F.E. solver and later coupled with the ship collision S.E. solver *SHARP* [32].

Using the 2$^{\text{nd}}$ Newton's law, the equation of a grounded ship movement may be written as [41]:

$$\underline{\underline{M}}[\dot{y}] + \underline{\underline{G}}[y] = [F_C(x)] + [F_W(y,x)] + [F_H(y,x)] + [F_V(y,x)] \tag{14}$$

Here, vector x denotes the position of the ship centre of gravity (CoG) with respect to the earth-fixed coordinate system while vector y denotes its absolute body-fixed velocity. $\underline{\underline{M}}$ is the mass matrix, defined as the sum of rigid body and water added mass matrices, while the gyroscopic matrix $\underline{\underline{G}}$ is defined as the sum of rigid-body and water added gyroscopic matrices.

The right hand side of Eq. 14 includes external forces and moments that apply on the ship's hull:

- $[F_C(x)]$ is the vector of contact force/moment exerted by the rock on the ship and expressed at the ship's CoG.
- $[F_W(y,x)]$ and $[F_V(y,x)]$ are the wave radiation and drag damping force/moment vectors respectively.
- $[F_H(y,x)]$ is the hydrostatic restoring force/moment vector.

Starting from the ship hydrodynamic characteristics (water added mass, restoring stiffness, wave and drag damping) calculated by a seakeeping code and provided in a matrix form, *MCOL* solver calculates the hydrodynamic loads F_H, F_V, and F_W and solves Eq. 14 for y and its derivative. More details about *MCOL* solver may be found in [41, 42].

2.6 FLAGS/MCOL coupled tool

Based on the flowchart presented in Figure 1, the overall functioning of *FLAGS/MCOL* tool may be summarised as follows:

1. Input - Input files containing the S.E mesh, ship hydrodynamic properties, rock parameters and grounding scenario data are read.
2. Detection - At each time step, the super-elements impacted by the rock are identified and the rock penetration into each super-element is computed.
3. Internal mechanics - Then, for each super-element and depending on its type (bottom/double bottom, floor, girder or floor/girder intersection in bottom grounding ; side shell, deck, bulkhead or deck/bulkhead intersection in side grounding) and whether the outer shell is ruptured or not, the resisting force is computed using the closed-form expressions derived for paraboloid shaped rocks and reported in *Pineau et al.* [17] and *Pineau et al.* [18].
4. External dynamics - By summing the contribution of each impacted element, the total resisting forces acting along longitudinal, transverse and vertical directions as well as resulting moments with respect to the ship CoG are computed. Forces and moments are then transferred to *MCOL* program which solves Eq. 14. The new position of the ship CoG as well as the roll, pitch and yaw angles are calculated and transferred back to *FLAGS* solver for the next iteration.

5. Stopping criteria - The program terminates as soon as a stop criterion is satisfied, otherwise all S.E. positions are updated, the time step is eventually recalculated based on the current ship velocity V_x and another iteration begins.

3 Results

3.1 Bottom grounding

In a first step, *FLAGS/MCOL* S.E. solver has been validated in bottom grounding situations through a benchmark carried out by three partners of *FLARE* project, namely Aalto University in Finland, Strathclyde University (MSRC[2]) in Scotland and ICAM Engineering School in France. As this benchmark has already been reported in [33] and [43], only main data and results are described in this subsection.

The Floodstand cruise ship B [44] has been selected to compare different modelling approaches and her bottom structure has been simplified to avoid some geometric uncertainties due to the complex real scantling - see Figure 4. Her main particulars are listed in Table 1. The simplified structure is composed of a bottom, a double bottom, floors and girders and its main particulars are given in Table 2. Note that the ship bow was represented by an inclined bottom plating located at the fore part of the model and making an upward angle of 35° with a horizontal plane.

Parameters	Floodstand ship B
Overall length (m)	238
Moulded breadth (m)	32.2
Depth (m)	16
Design draft (m)	7.2
Displacement (tonne)	34 000

Table 1: Main particulars of Floodstand ship B

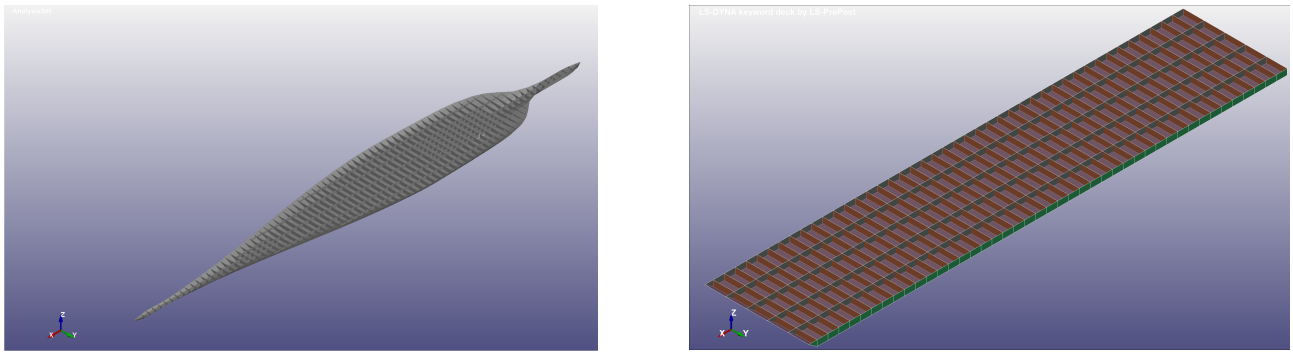

Figure 4: Floodstand ship B bottom - left (real) - right (simplification)
- Source: [43]

Two impact locations were considered, the first at the centre line, i.e., $y = 0$ (Centred impact) and the second at $y = B/4 = 7.125\,m$ from the centre line (Off-centred impact). The ship was given an horizontal surge velocity of 5 knots ($\approx 2.572\,m/s$) and a friction coefficient $\mu = 0.3$ was set between the structure and the rock. Regarding the latter, coefficients C and E were set to 3.7 and 6 respectively in order to represent a sharp rock - see Figure 5. The impact height was set to $2m$ in order to trigger the rupture of both the bottom and double bottom.

[2]Maritime Safety Research Centre

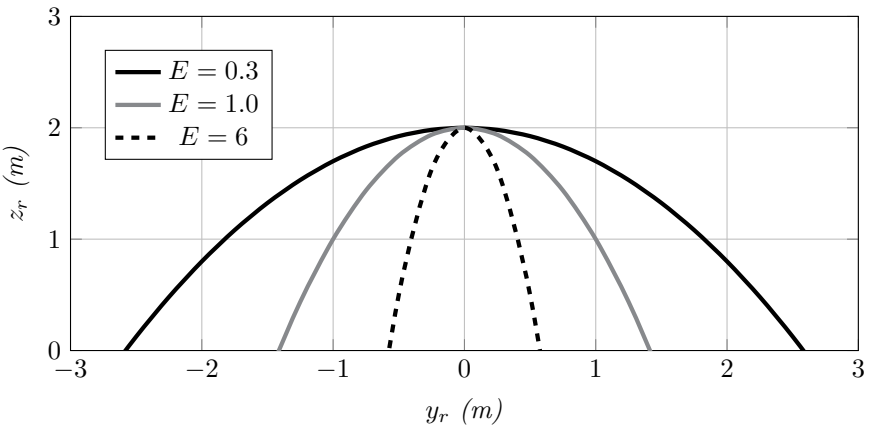

Figure 5: Transverse cut - Rock shape

Description	Dimensions
Length (m)	130
Breadth (m)	28.5
Double bottom height (m)	1.6
Transverse frame spacing (m)	3
Longitudinal girder spacing (m)	5.7
Outer bottom thickness (mm)	15
Inner bottom thickness (mm)	10
Transverse floor thickness (mm)	15
Longitudinal girder thickness (mm)	20

Table 2: Simplified bottom structure main characteristics - Bottom grounding benchmark

Aalto and MSRC performed numerical analyses using *Ls-Dyna/MCOL* finite element software. A rigid perfectly plastic material behaviour law and a $80mm$ element-size mesh were used by Aalto while MSRC considered a modified true stress-strain curve as proposed by *Paik & Thayamballi* [45], with a $250mm$ element size mesh.

The evolution of the dissipated energy as a function of the breach length obtained by Aalto and MSRC are compared in Figure 6 with the results post-processed from *FLAGS/MCOL* simulations. In addition, the damage extent and dissipated energy post-processed from Aalto and MSRC numerical simulations are compared to *FLAGS* results in Table 3.

The discrepancy observed on the damage extent retrieved from F.E. simulations is mainly due to the different mesh sizes used by Aalto and MSRC. The deviation with S.E. results mainly comes from the assumptions made when deriving closed-form expressions. First, the material is assumed as rigid perfectly plastic in *FLAGS*, while hardening was considered by MSRC when setting elastic-plastic behaviour laws in *Ls-Dyna* models. Second, several assumptions were made on the deformation mechanisms implemented in the S.E. solver for raking grounding [17] simulations, which mainly explains the discrepancies with F.E. results. Nevertheless, both Figure 6 and Table 3 show the very good performance of the S.E. approach to estimate the breach length, keeping in mind that *FLAGS* computation time is around 4 minutes, while around 4 days were required to complete F.E simulations using parallel computing.

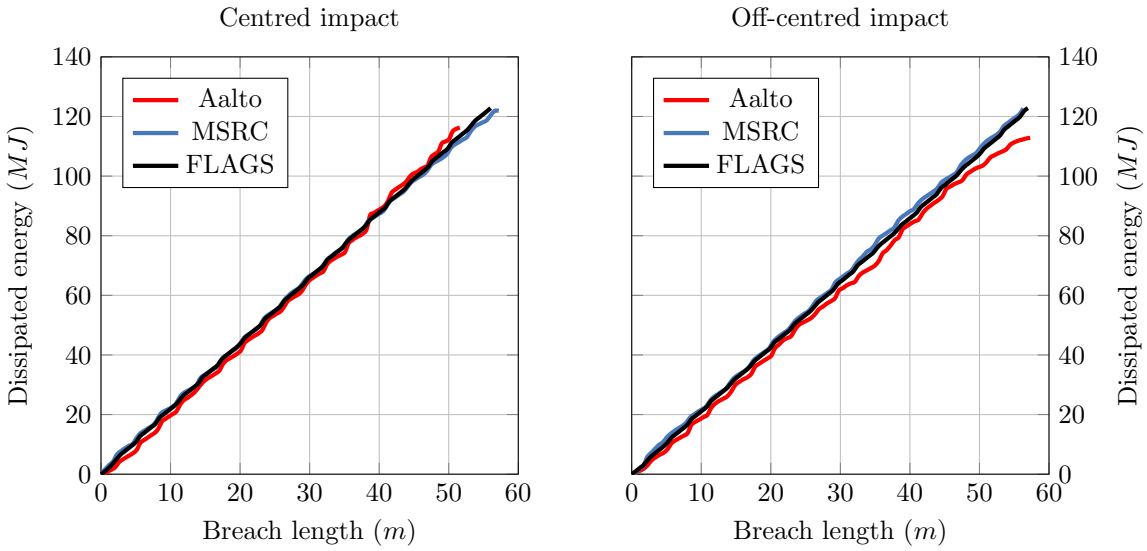

Figure 6: Dissipated energy versus breach length - Retrieved from [33]

Scenario	Partners	Damage length (m)	Dissipated energy (MJ)	Deviation damage length	Deviation dissipated energy	Computation time
Centred	FLAGS	56.0	122.8	—	—	4 minutes
	Aalto	51.6	116.3	-7.9%	-5.3%	4 days[3]
	MSRC	57.2	121.9	2.1%	-0.8%	—
Off-centred	FLAGS	57.0	122.8	—	—	4 minutes
	Aalto	57.3	112.9	0.6%	-8.1%	4 days
	MSRC	56.3	122.7	-1.1%	-0.1%	—

Table 3: Bottom grounding benchmark synthesis - Retrieved from [33]

The major advantage of the S.E. solver is its rapidity, only 4 minutes were necessary to complete one simulation with *FLAGS/MCOL* for a discrepancy on the damage extent that does not exceed 8%. Further validations with different rocks and different ships are obviously needed to consolidate the reliability of the developed program but these first results obtained on a full scaled ship structure were very encouraging regarding both the precision and computation time.

3.2 Side grounding

In a second step, the reliability of *FLAGS/MCOL* has been verified for side grounding situations against Ls-Dyna finite element calculations. For this purpose, the simplified side section extracted from *Floodstand ship B* cruise ship [44] and depicted in Figure 7 was considered. The model, which includes a side shell, decks and transverse bulkheads, is $58m$ long and $16m$ wide. The fore part of the side shell makes an angle $\alpha = 12.7°$ with respect to the ship longitudinal axis and represents a portion of the ship bow. The spacing between transverse bulkheads and between decks is $15m$ and $2.8m$ respectively. Table 4 gives the thickness of the different sub-structures.

[3]Computation time obtained using 8 SMP thread on Intel Xeon CPU E5-2680 V4 at 2.88 GHz

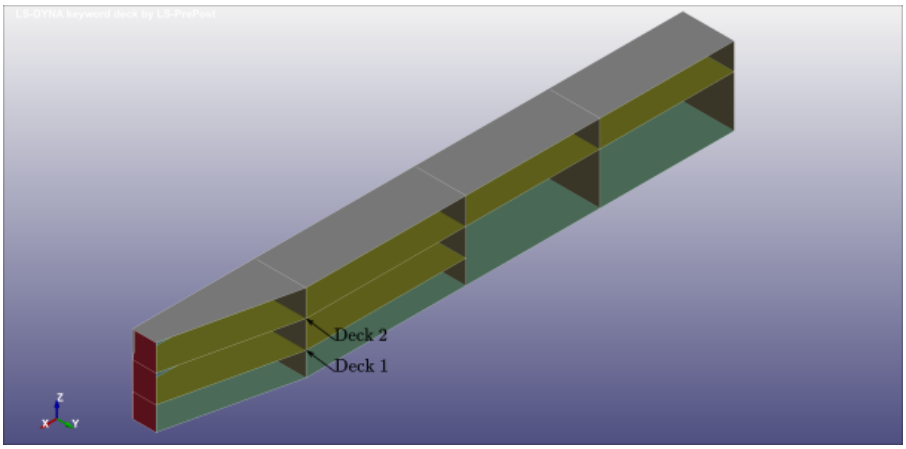

Figure 7: Side grounding ship benchmark model (without side shell)

Item	Thickness (mm)
Side shell	15
Inner Side	10
Transverse bulkheads	10
Deck	8

Table 4: Side grounding model : component thickness

In *Ls-Dyna* F.E. model, the structure was meshed using Belytschko-Tsay shell elements [46] with a size of $30mm$ and 5 integration points through thickness, according to the calibration carried out by comparison with experimental results and detailed in *Pineau et al.* [18]. A bi-linear elastic-plastic behaviour law was adopted for the mild steel material with the characteristics listed in Table 5. Above-mentioned calibration also allowed to show that a classical shear criterion may be used to capture the components rupture. Following the method proposed by *Scharrer & Zhang* [47], the failure strain threshold value was calculated as:

$$\varepsilon_{fail} = 0.056 + 0.54\frac{t_h}{l_e} \tag{15}$$

Where t_h is the component thickness (Table 4) and l_e the element size.

Material properties		
Yield stress	σ_y *(MPa)*	240
Poisson's ratio	ν	0.33
Density	ρ (kg/m^3)	7850
Young modulus	E_{young} *(MPa)*	210 000
Tangent modulus	E_{tan} *(MPa)*	1018

Table 5: Mild steel properties

Three side grounding scenarios were considered with the parameters summarised in Table 6. In the first one, the ship is supposed to impact a sharp rock between decks 1 and 2 (see Figure 7). In the second, the side shell impacts a medium rock at deck 1 level (see Figure 11) and the last scenario simulates an side impact against a large rock just above deck 1. The shape of the three different rocks considered in this study are shown in Figure 5. In Table 6, H refers to the initial rock penetration into the side shell, while Z denotes the initial vertical position of the rock apex with respect to the ship's bottom.

Scenario id	$H\ (m)$	$Z\ (m)$	$C\ (m^{-1})$	$E\ (m^{-1})$	$V_x\ (m/s)$
1	2	3.95	3.7	6	1.285
2	1.5	2.5	1	1	2.572
3	1.5	2.95	0.3	0.3	2.572

Table 6: Validation of side grounding solver - Scenario parameters

Longitudinal and transverse resisting forces as well as dissipated energies are plotted in Figures 8, 9 and 10 as a function of the damage extent, i.e. the contact distance (raking distance) as the hull-rock interaction proceeds in time, while Table 7 provides both the total dissipated energies and final damage extents post-processed from numerical (*Ls-Dyna/MCOL*) and analytical (*FLAGS/MCOL*) calculations.

Figures 8 to 10 show a relatively good agreement between numerical and analytical results, even if the longitudinal resisting force is slightly underestimated by *FLAGS/MCOL*. The highest discrepancies are observed in scenario n^{o} 2, in which the rock impacts the side shell at deck 1 level. It is observed from *Ls-Dyna* F.E. simulation that side shell failure occurs just above the junction with the deck, as illustrated in Figure 11. Resulting vertical force F_V pushes the ship downward. As a consequence, the impacted deck is subjected to bending rather than concertina splitting and the side shell below the deck also deforms, dissipating additional energy. Such deformation modes were not considered when deriving analytical solutions (see *Pineau et al.* [17]) and this may explain the discrepancy observed on both the resisting forces and dissipated energy.
All in all, Table 7 shows that the damage extent given by numerical and analytical solutions are in pretty good agreement, the discrepancy not exceeding 13%.

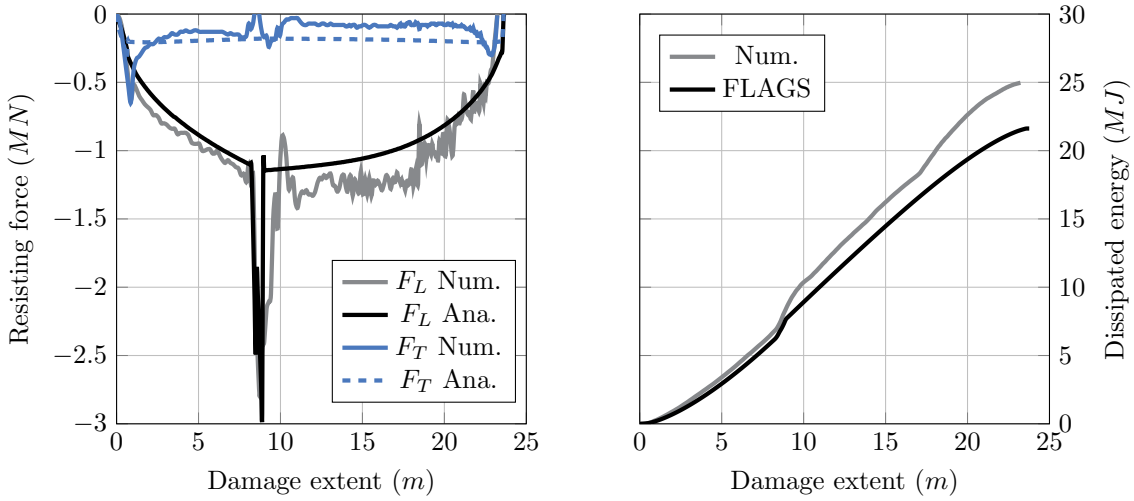

Figure 8: Side grounding benchmark - scenario 1

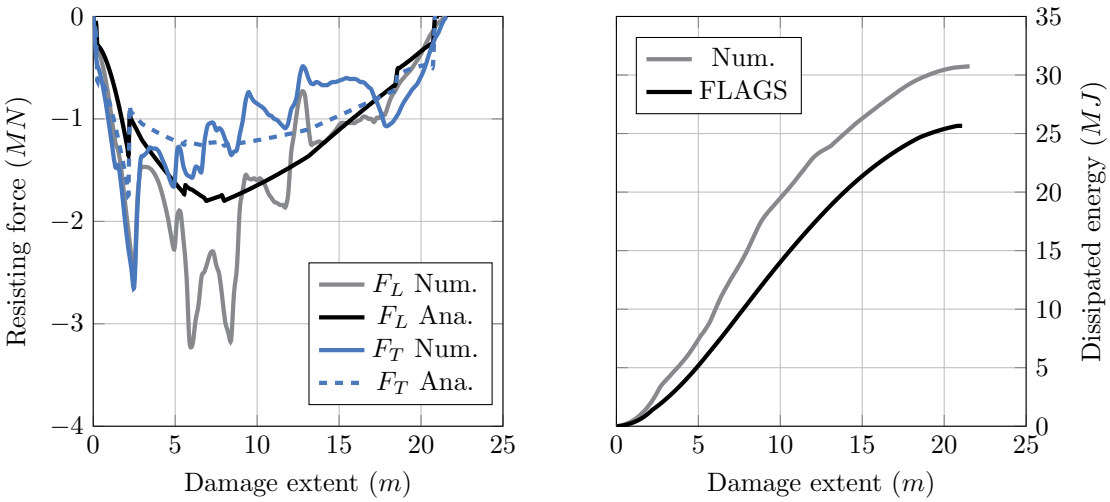

Figure 9: Side grounding benchmark - scenario 2

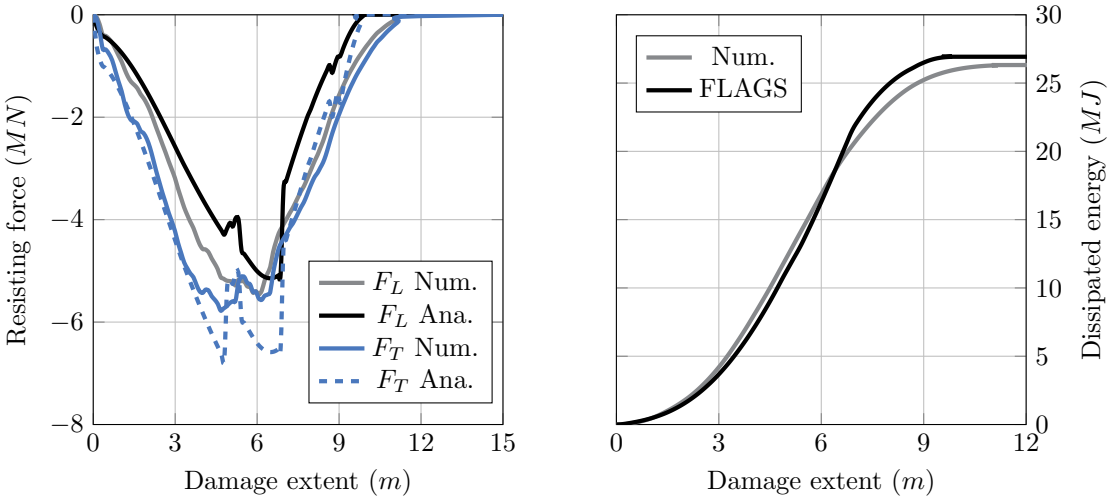

Figure 10: Side grounding benchmark - scenario 3

Scenario id	Dissipated energy Num. (MJ)	Dissipated energy Ana. (MJ)	Damage extent Num. (m)	Damage extent Ana. (m)	Deviation energy	Deviation damage
1	24.97	21.62	23.23	23.54	13.42%	-1.33%
2	30.74	25.66	21.55	21.1	16.5%	2.1%
3	26.32	26.93	11.37	9.93	-2.3%	12.6%

Table 7: Side grounding benchmark - Overall dissipated energy and damage extent

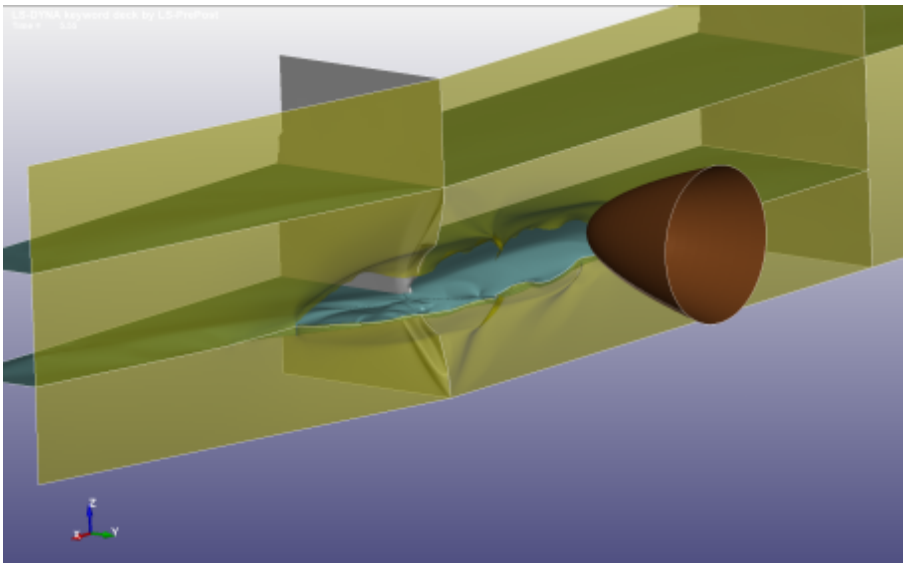

Figure 11: Side grounding - Scenario 2

For each scenario, it was also observed that the transverse reaction force F_T exerted by the rock pushed the ship away from the rock, as illustrated in Figure 12. Resulting ship sway and yaw motions led to a progressive decrease of the rock penetration until the contact was totally lost.

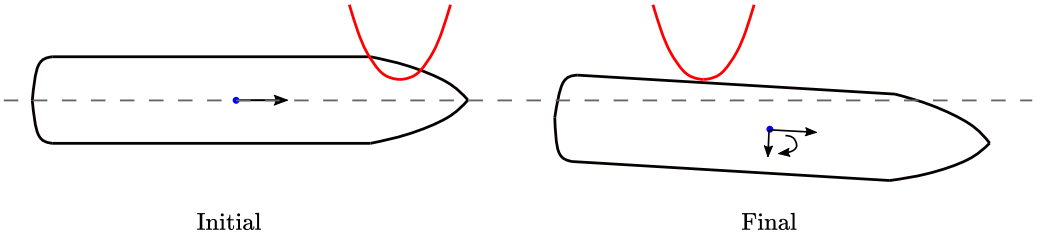

Figure 12: Ship side grounding: initial and final position

In scenario n^o 3, the rock penetrated the hull over $1.5m$ at the beginning of the impact. When the contact was lost, the displacement of the centre of gravity along the sway direction was $1.22m$, the yaw angle close to 0° and the roll angle $\approx 5^\circ$. Neglecting the roll motion would have resulted in longer damage extent. One may thus conclude that the ship is not restrained to an in-plane motion but its 6 degrees of freedom have actually to be considered in external dynamics calculation.

Several conclusions can be drawn from this validation work:

1. Both forces F_L and F_T play an important role in side grounding situation, unlike bottom grounding in which the damage extent is mostly governed by the longitudinal resisting F_L. Similarly to bottom grounding, F_L has for effect to decrease the ship surge velocity and to dissipate a large amount of energy, while F_T causes sway, yaw and even roll rigid body motions of the ship. The hull is pushed away from the rock, reducing drastically the damage extent compared to bottom grounding.

2. Out-of-plane rigid body motions must also be considered in such analysis as the ship is not limited to surge, sway and yaw motions.

3. The simplified tool allows to complete one simulation in around 40 seconds, while the average computation time for one scenario is about 110 hours with *Ls-Dyna/MCOL*. *FLAGS/MCOL* thus appears to be around 10 000 times faster, with an average discrepancy on dissipated energy and damage extent equal to 10.6% and 5.3% respectively.

4 Parametric grounding analyses

4.1 Methodology

Thousands of grounding scenarios were then simulated to investigate the influence of different parameters on the ship damage extent, taking advantage of the speed of *FLAGS/MCOL*. The objective was to focus on the structural improvements of a given structure. Grounding scenarios involving a reference ship design and an improved one regarding the crashworthiness were run without considering the probability of the accident. The influence of the alternative scantling on the damage extent was then evaluated. Example of application of such methodology may be found in *Conti et al.* [48] for ship-ship collision analysis. The principle of the method may be summarised as follows:

1. First, a series of grounding simulations are performed on the original ship configuration, varying the rock shape as well as the ship impact location, initial velocity and penetration. Then, for each scenario, the damaged extent L_0 is post-processed.
2. All the simulations are then rerun after changing only one structural parameter, the outer shell thickness for instance, and the damage extent L_N related to the ship's new design is post-processed.
3. The damage extent L_N is finally compared to the initial damage L_0 and the effect of the structural modification is quantified through a breach reduction factor $k_b = \frac{L_N - L_0}{L_0}$.

An (averaged) effective breach reduction factor $\overline{k_b}$ is finally calculated as:

$$\overline{k_b} = \frac{1}{N} \sum_{i=1}^{N} k_{bi} \tag{16}$$

Where N is the number of grounding scenarios that have been investigated. As recently demonstrated by *Conti et al.* [48], a large number of scenarios have to be considered to obtain reliable conclusions because the influence of a reinforcement can greatly depend on the grounding scenario. A direct consequence is that the grounding scenarios shall be chosen so as to lead to realistic damages, when compared to real accidents.

In following two subsections, we present the sensitivity analyses carried out for ship bottom grounding and side grounding events respectively.

4.2 Bottom grounding

4.2.1 Effect of structural modifications

First, the influence of structural modifications on ship bottom damage extent was investigated considering the Floodstand cruise ship B model depicted in Figure 4. For each structural modification, 540 scenarios resulting from all the combinations of the parametric values listed in Table 8 were simulated.

	Parameters	Values
Rock	C (m^{-1})	0.3 - 0.5 - 1.0 - 1.5 - 3 - 6
Parameters	E (m^{-1})	0.3 - 0.5 - 1.0 - 1.5 - 3 - 6
Impact	Y (m)	0 - 2.85 - 7.125
Position	Z (m)	0.3 - 0.5 - 1 - 2 - 3
Initial surge velocity	V_x (m/s)	2.572

Table 8: Scenario parameters - Bottom grounding analysis

Above values were defined considering the following situations. First, according to *Youssef & Paik* [49], the lateral position (Y) of the impact follows a uniform distribution law. Three positions were therefore selected in such a way that the impact is located between 2 girders ($Y = 0$), affects partially one girder ($Y = 7.125$) and is located just below a girder ($Y = 2.85$). Second, vertical positions (Z) of the rock apex with respect to the ship bottom were chosen to simulate both sliding and raking situations: small penetrations enable sliding grounding while large penetrations will foster raking grounding and, for the highest values, inner hull crushing. Finally, following the work of *Conti* [50], the rock parameters were selected to consider a large variety of rock shapes,

from shallow ($E = 0.3$) to sharp ($E = 6$) rocks.

Following above methodology, the sensitivity analysis was focused on the following structural parameters:

- Outer bottom thickness (t_{hO})
- Inner bottom thickness (t_{hI})
- Floor thickness (t_{hF})
- Girder thickness (t_{hG})
- Material flow stress (σ_0)

Each parameter was changed by ±25% and ±50% from its initial value. Combining five values for each parameter with the aforementioned 540 scenarios led to 11 340 grounding simulations. It should be stressed here that the structural modifications were supposed not to alter the hydrodynamic properties of the ship. Indeed, the change in mass was shown to be negligible compared to the total ship mass.

A typical example of results obtained when analysing the influence of the outer shell thickness is depicted on Figure 13.

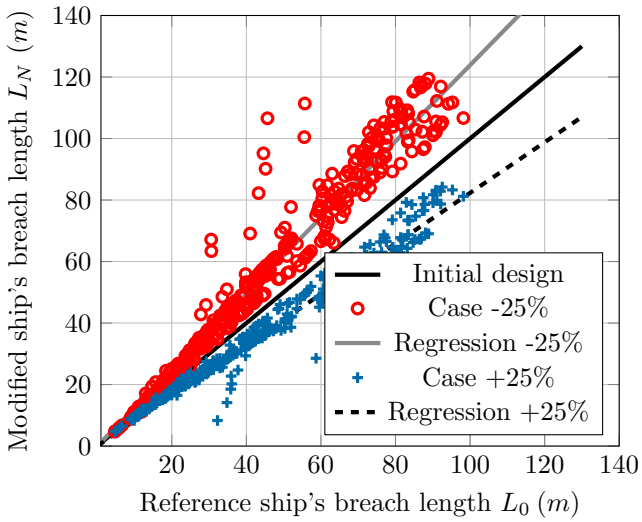

Figure 13: Evolution of the breach length when the outer shell thickness is varied

Table 9 presents the effective reduction factors $\overline{k_b}$ post-processed from the 11 340 simulations. Note that in order to compare like with like, the scenarios for which the damage extent equalled the ship length ($130m$) were removed from the analysis.

	Case -50%	Case -25%	Case +25%	Case +50%
Parameter	$\overline{k_b}$	$\overline{k_b}$	$\overline{k_b}$	$\overline{k_b}$
Outer bottom thickness t_{hO}	+49.0%	+28.6%	-21.9%	-29.4%
Inner bottom thickness t_{hI}	+12.5%	+8.35%	-6.8%	-20.37%
Transverse floor thickness t_{hF}	+1.0%	+0.6%	-0.6%	-6.32%
Longitudinal girder thickness t_{hG}	+25.0%	+21.7%	-14.3%	-18.8%
Flow stress σ_0	+88.5 %	+29.0%	-18.0%	-29.1 %

Table 9: Effective breach reduction factors - Bottom grounding

We denote by F_L and F_m the averaged longitudinal resisting force related to reference ship and modified ship design respectively. We also denote by τ the ratio:

$$\tau = \frac{F_L}{F_{Lm}} \tag{17}$$

The average force on the modified ship design is thus equal to τF_L.

We further assume that the entire ship initial kinetic energy E_0 has been dissipated during the grounding event. The theoretical breach reduction factor λ may be estimated as:

$$\lambda = \frac{E_0/(\tau F_L) - E_0/F_L}{E_0/F_L} = \frac{1}{\tau} - 1 \tag{18}$$

According to the closed-form expressions derived from limit plastic analysis and reported in [17], increasing the flow stress σ_0 by 25% leads to an increase of the resistance force F_L by 25%, i.e. $\tau = 1.25$. Application of Eq. 18 for different values of σ_0 is plotted on Figure 14 in addition to results obtained from *FLAGS*. One can show that Eq. 18 provides a good estimation of the effect of the parameter in bottom grounding.

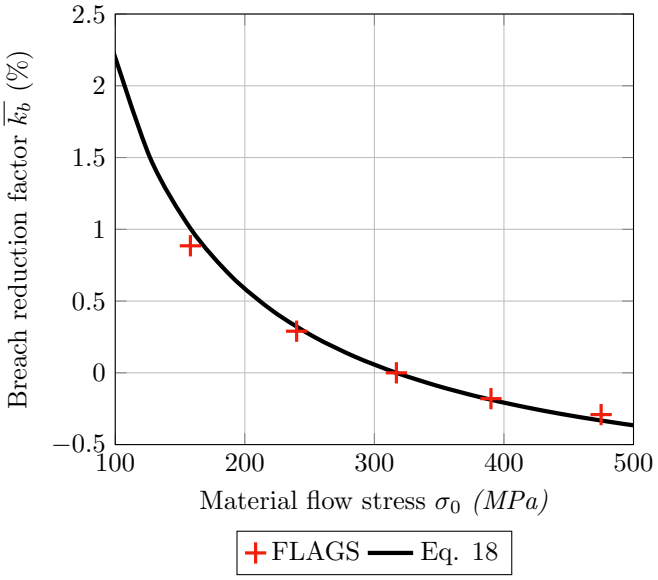

Figure 14: Evolution of the breach reduction factor $\overline{k_b}$ with the material flow stress σ_0

More generally, several conclusions may be drawn from the analysis of Table 9:

1. In the great majority of scenarios, the ship moves along a straight path meaning that the hydrodynamic effects other than the ship surge added mass are very limited. Therefore, in the considered bottom grounding scenarios, the calculations stopped either because the initial kinetic energy was entirely dissipated or because the ship was damaged along its full length ($130m$).

2. As expected, since the contribution of transverse floors is limited, varying the floor thickness by $\pm 25\%$ and even $\pm 50\%$ has a marginal influence on the damage extent.

3. The effect of the inner bottom thickness on the damage extent is also rather limited. In fact, the inner bottom was observed to be crushed in only 40% of the scenarios. Moreover, when the inner bottom was impacted by the rock, it contributed by only 25% to the dissipation process.

4. The material flow stress σ_0 has the major influence on the damage extent of the damage, followed by outer shell thickness t_{hO} and girder thickness t_{hG}.

5. The damage extent does not vary linearly with the scale factor τ but rather in $1/\tau$.

4.2.2 Effect of friction

The friction coefficient between the rock and the vessel is often arbitrarily set to $\mu = 0.3$ - see for instance [8, 13, 14, 28]. To quantify its effect on the damage extent, 1080 additional grounding simulations with a friction coefficient set either to $\mu = 0.1$ or to $\mu = 0.6$ were carried out and the results are plotted in Figure 15.

As expected, damage length and friction coefficient vary inversely. However, it is noteworthy that by only decreasing μ from 0.3 to 0.1, the damage extent is increased by almost 50%. This highlights once again the

large amount of energy that is dissipated through friction in a bottom grounding event but also the importance of systematically investigating the influence of this parameter.

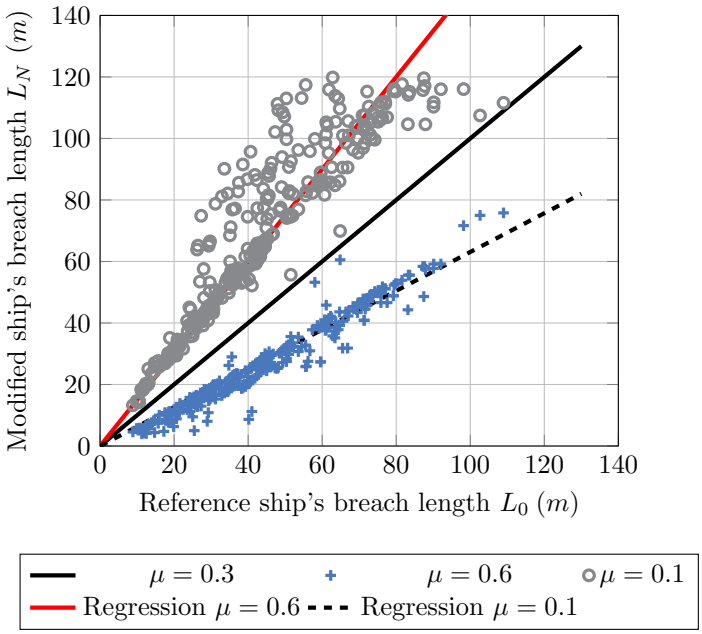

Figure 15: Influence of μ on the damage length - Bottom grounding

4.2.3 Conclusion regarding bottom grounding parametric analysis

Thousands of ship bottom grounding scenarios have been simulated using *FLAGS/MCOL* tool with the objective to investigate the influence of structural modifications and friction coefficient on resulting breach size.

It transpired from this analysis that the three most influencing structural parameters are the outer bottom thickness, the girder thickness and the steel flow stress, suggesting that a reinforcement strategy could be to increase outer shell or girder thickness or select a higher steel grade (higher flow stress). However, increasing the thicknesses would also increase the ship mass, as well as the production cost. In fact, as the Floodstand ship B is concerned, increasing the outer shell thickness by 25% allows to reduce the damage extent by almost 20%, for an additional mass of around 110 tonnes, which corresponds to less than 0.5% of the total ship mass.

The damage extent does not vary linearly with the parameter scale factor τ but rather in $1/\tau$. Of course, other parameters such as transverse bulkheads or girder spacing as well as contribution of longitudinals could also be investigated. Recently, using *FLAGS/MCOL*, *Conti* [50] found that doubling the number of girders has the same effect as increasing by 25 % the material flow stress i.e., $\overline{k_b} \approx 20\%$.

The strong effect of friction on the damage extent was also demonstrated. This means that in a grounding analysis aiming to predict the outer/inner shell opening, as the friction coefficient between the rock and the ship hull cannot be known in advance, it is of paramount importance to study its influence on the results.

4.3 Side grounding

4.3.1 Effect of structural modifications

As for bottom grounding, a sensitivity analysis of the damage extent to ship side structural modifications was then carried out. The same methodology was used but the varied structural parameters were the following ones:

- Side shell thickness (t_{hS})
- Inner deck thickness (t_{hI})
- Transverse bulkhead thickness (t_{hB})
- Material grade (σ_0)

The 140m long and 16.1m wide ship model used for the parametric analysis is depicted on Figure 16 (without side shell). Indeed, this is the overall Floodstand B cruise ship side that was geometrically simplified. Its main characteristics are given in Table 10.

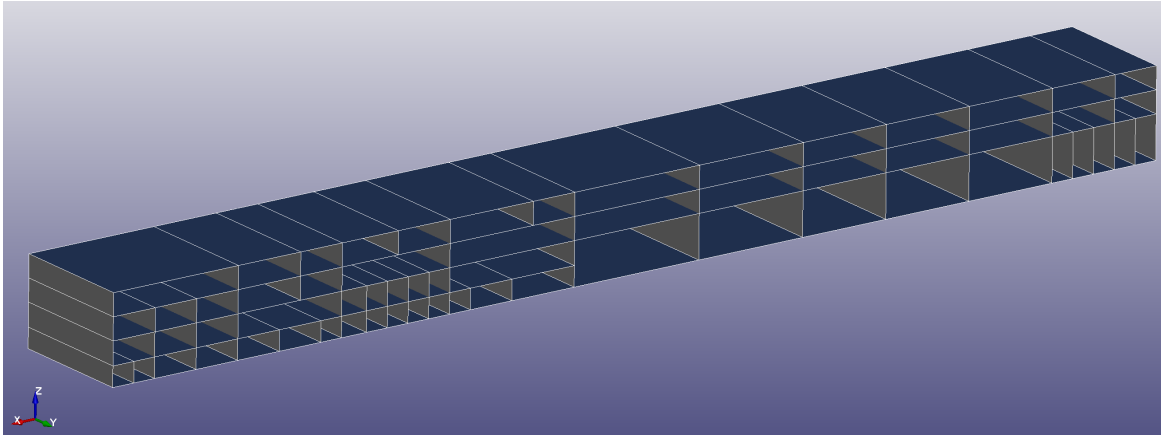

Figure 16: S.E. model used in side grounding parametric analysis (view without the side shell)

Element	Thickness (mm)
Side Shell	15
Mid decks ($z = 4.1m$ and $z = 7m$)	10
Upper decks ($z = 9.8m$ and $z = 12.6m$)	8
Transverse bulkheads, below $z = 7m$	11
Transverse bulkheads, above $z = 7m$	8

Table 10: Sub-structures thickness - Side grounding parametric analysis

For each alternative design, 540 simulations were carried out taking into account all the combinations of the values listed in Table 11.

Parameters	Values
C (m^{-1})	0.3 - 0.5 - 1.0 - 1.5 - 3 - 6
E (m^{-1})	0.3 - 0.5 - 1.0 - 1.5 - 3 - 6
H (m)	0.3 - 0.5 - 1 - 2 - 3
Z (m)	5.55 - 7 - 9
V_{surge} (m/s)	2.572 - 5.0

Table 11: Scenario parameters - Side grounding parametric analysis

The relevance of these values may be checked by comparing the breaches retrieved from *the damage length* simulations with actual breaches that have been extracted from real grounding events as part of EMSA3 European research project [51]. One may observe in Appendix D that EMSA3 damage domains are pretty well populated by *FLAGS/MCOL* results.

In total, 18 360 scenarios were simulated varying t_{hS}, t_{hI}, t_{hB} and σ_0 by $\pm 50\%$ from their initial value. Resulting effective breach reduction factors $\overline{k_b}$ are given in Table 12.

	Case -50%	Case -25%	Case +25%	Case +50%
Parameter	$\overline{k_b}$	$\overline{k_b}$	$\overline{k_b}$	$\overline{k_b}$
t_{hS}	+39.6%	+14.0%	-11.0%	-18.55%
t_{hI}	+20.0%	+10.0%	-11.0%	-13.58%
t_{hB}	+0.007%	+0.005%	-0.009%	-0.021%
σ_0	+40.3 %	+15.0%	-12.0%	-16.8 %

Table 12: Synthesis of the side parametric analysis

One may observe from this table that:

1. Varying the thickness of transverse bulkheads does not affect the damage extent.
2. Unlike bottom grounding, varying side shell thickness or material grade has almost the same effect on the damage extent.
3. The effect of a structural modification is much less pronounced compared to bottom grounding. For instance, in bottom grounding, when the material flow stress σ_0 was changed by $\pm 25\%$, the damage length was also modified by $\approx \pm 25\%$. However for side grounding, the damage extent varied by only $\approx \pm 13.5\%$ in average, i.e. around two times less.

In order to explain this last point, let us assume that the ship motions are limited to sway and surge (yaw is neglected for simplification). The second Newton's law writes:

$$\begin{cases} \ddot{x}(t) = -\tau \frac{F_L}{M_L} \\ \\ \ddot{y}(t) = \tau \frac{F_T}{M_T} \end{cases} \tag{19}$$

Where M_L and M_T are the ship mass plus the added mass along surge and sway direction respectively, F_L and F_T are the resisting forces acting and τ traduces the increase or decrease of the resisting force related to the modified structure. Solving Eq. 19 by considering the ship initial surge velocity v_{x0} gives:

$$\begin{cases} x(t) = -\frac{\tau}{2} \frac{F_L}{M_L} t^2 + v_{x0} t \\ \\ y(t) = \frac{\tau}{2} \frac{F_T}{M_T} t^2 \end{cases} \tag{20}$$

Now, let us further assume that the breach is limited by the sway motion of the ship. In this case, the calculation stops once the ship has undergone a sway displacement equal to the initial rock penetration H, which is achieved within a time t_f:

$$t_f = \sqrt{\frac{2HM_T}{\tau F_T}} \tag{21}$$

Injecting Eq. 21 into Eq. 20 allows to estimate the damage extent:

$$L(\tau) = -\frac{F_L M_T}{F_T M_L} H + v_{x0} \sqrt{\frac{2HM_T}{\tau F_T}} \tag{22}$$

Resulting theoretical reduction factor λ thus writes:

$$\lambda = \frac{L(\tau) - L(1)}{L(1)} \tag{23}$$

Unfortunately Eq. 23 does not lead to a simple form as in Eq. 18. However, with the expected resisting forces and ship inertia, one can show (see Appendix B) that λ is bounded by:

$$1.2 \left(\frac{1}{\sqrt{\tau}} - 1 \right) \leq \lambda \leq \frac{1}{\sqrt{\tau}} - 1 \tag{24}$$

Application of Eq. 24 for different values of σ_0 is plotted on Figure 17 in addition to numerical results. One can show that the theoretical method is in accordance with the numerical results. The slight variation may be due to the fact that yaw and roll motions have been neglected in above reasoning. Therefore, the effect of reinforcement in side grounding is proportional to $1/\sqrt{x}$.

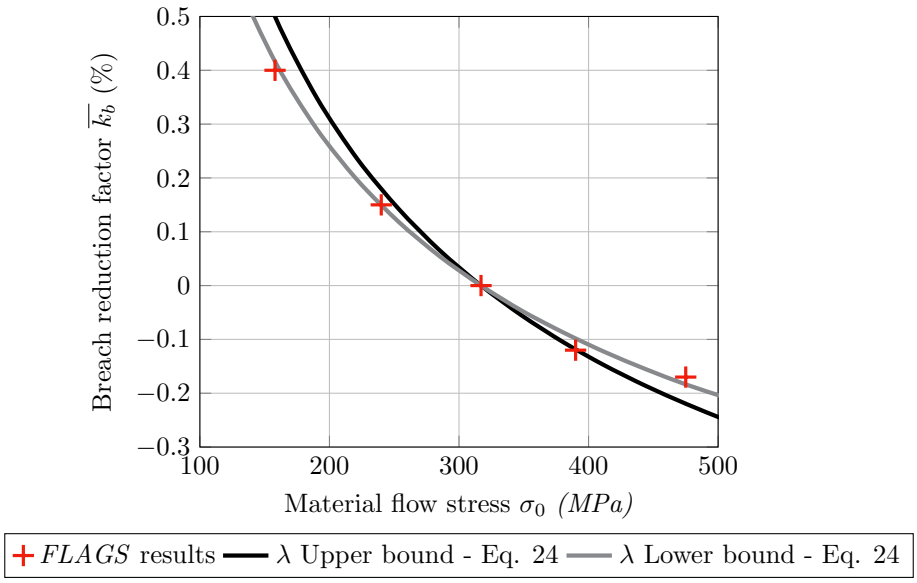

Figure 17: Evolution of breach reduction factor $\overline{k_b}$ with material flow stress σ_0 - Side grounding

Finally, using Eq. 18 and Eq. 24, the theoretical breach reduction factor for side and bottom grounding is plotted as a function of τ in Figure 18.

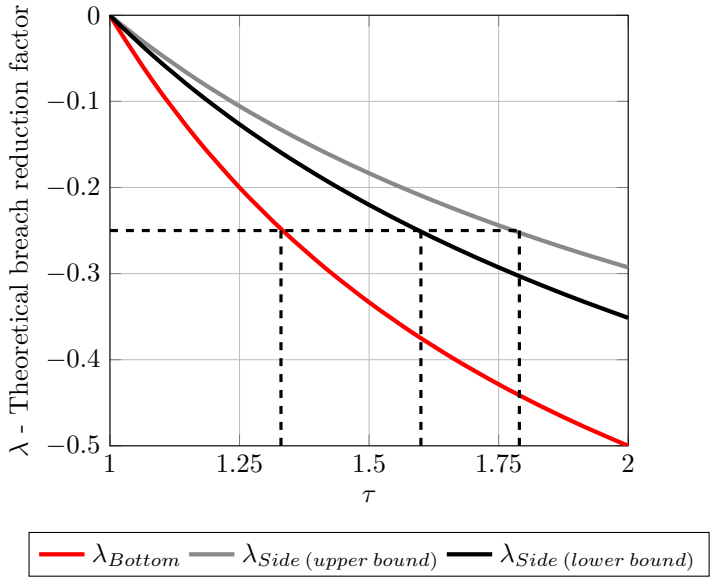

Figure 18: Evolution of the theoretical breach reduction factor with τ in Bottom and Side grounding

This figure shows that the effect of a structural reinforcement on the damage extent will be always lower in side grounding than in bottom grounding. For instance, if one wishes to decrease the damage extent by 25% in both bottom and side grounding, then the average resisting force should be increased by 33% in bottom grounding and 70% in side grounding. For more details please refer to Appendix C.

4.3.2 Effect of friction

As for bottom grounding, the effect of friction on the ship side damage length is now investigated. For this purpose, simulations are once again carried out considering three friction coefficients: 0.1, 0.6 and 0.3, this later being the reference.
Figure 19 illustrates the effect of this coefficient on the breach length. As shown by the figure, the friction coefficient does not have a significant influence on the damage length (less than 2%) since the ship rapidly moves away from the rock. One can thus conclude that unlike bottom grounding, friction is not a determining factor in side grounding analysis.

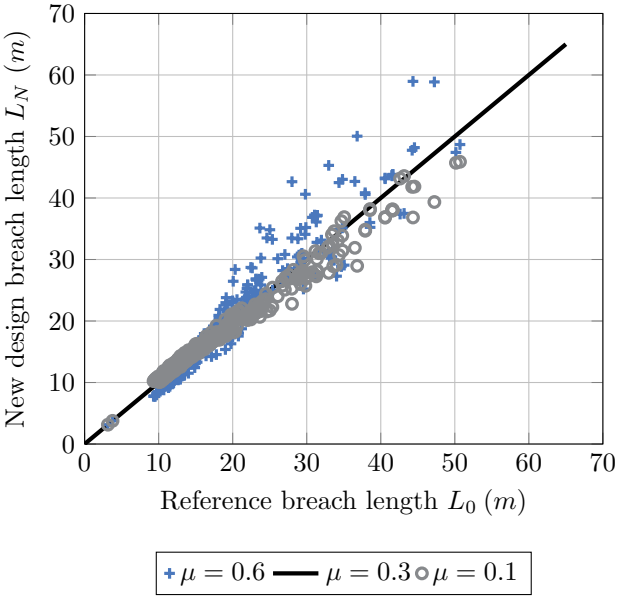

Figure 19: Influence of μ - Side grounding

4.3.3 Effect of initial kinetic energy

In bottom grounding, the damage extent is directly related to the ship initial kinetic energy (i.e. the velocity squared) but the question arises in side grounding. Side grounding scenarios are thus rerun on the reference design varying the initial velocity of the ship and the results in term of dimensionless damage extent are depicted in Figure 20.

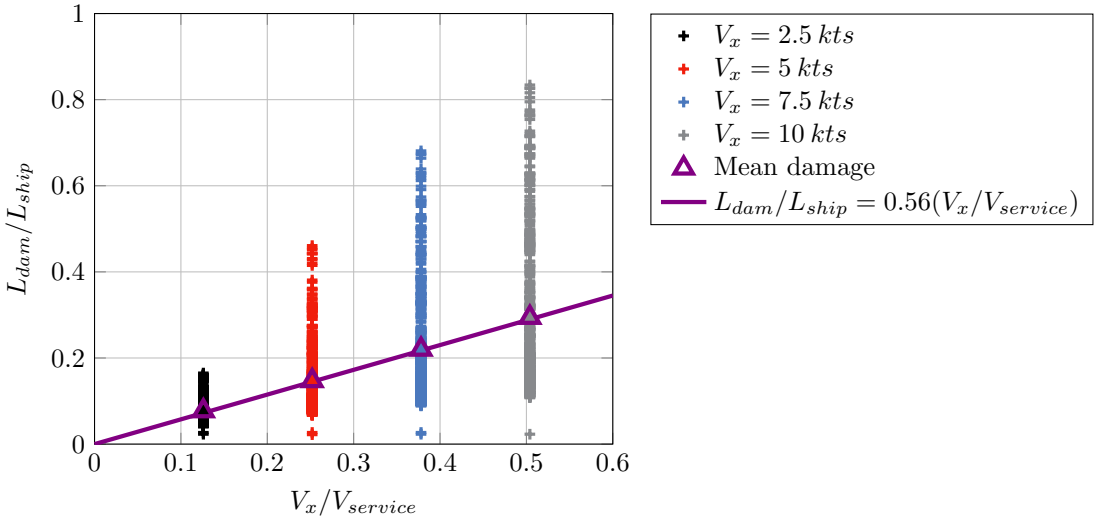

Figure 20: Damage length dependency on ship initial speed - Side grounding

As expected, the damage length increases with the initial surge velocity. Nevertheless, Figure 20 clearly indicates a linear dependency between damage extent and surge velocity, while the relation is rather quadratic in bottom grounding. This is directly related to the tendency of the ship to "escape" from the rock in side grounding. Besides, such result is in accordance with Eq. 22.

4.3.4 Conclusion regarding side grounding parametric analysis

FLAGS/MCOL tool has been used to conduct a structural sensitivity analysis based on thousands of simulations of side grounding events and the following conclusions may be drawn:

1. Due to the transverse force exerted by the rock, the ship tends to "escape" from the later, which strongly limits the damage extent.

2. The most influencing parameters in damage reduction are the material flow stress as well as the side shell thickness.

3. The damage extent varies linearly with the initial ship velocity, unlike bottom grounding for which the relation is rather quadratic. This implies that damage extent will be always less important in side grounding than in bottom grounding, even if the ship side is less stiffened. Another consequence is that a reinforcement will always be more efficient in bottom grounding than in side grounding.

4. Effect of friction is negligible since it has only an influence of about 2% on the damage extent

It is worth noting that other reinforcement solutions have been investigated by *Conti* [52] with *FLAGS/MCOL* program. For example, it was demonstrated that installing a double hull has a limited effect on the damage extent: $\overline{k_b} \approx 10\%$. In fact, as the ship rapidly moves away from the rock, the contribution of this structure to the energy dissipation is limited in time.

5 Discussion

In this paper, a fast and reliable tool for ship grounding damage analysis has been presented. This tool couples a super-element solver named *FLAGS* developed in the frame of this work with the 6-DoF external dynamics program MCOL [53].

The validation of *FLAGS/MCOL* has been performed by confronting the results to *Ls-Dyna/MCOL* finite element simulations, considering both bottom and side grounding scenarios. A good correlation has been observed between finite element and analytical results. Indeed, the rapidity of the developed tool is illustrated in Table 13, where *Ls-Dyna* and *FLAGS* average computation times are compared. The mean deviation between numerical and analytical results is also given. It appears that a *FLAGS/MCOL* simulation is in average around 10 000 times faster than a *Ls-Dyna* solution based on a $30mm$ element size, while the mean discrepancies with numerical results remain acceptable regarding the simplifications made.

Grounding type	*Ls-Dyna* CPU time $(hours)$[4]	*FLAGS* CPU time $(minutes)$	*Ls-Dyna/FLAGS* CPU time ratio	Average deviation
Bottom	720	≈ 4	11 000	-4.0%
Side	110	<1	10 000	-10.6 %

Table 13: Comparison of CPU time and average deviation between *Ls-Dyna* and *FLAGS* calculations

It was also observed from finite element and super-element simulations that while the damage extent is mainly governed by the ship initial kinetic energy in bottom grounding, the transverse force exerted by the rock in side grounding significantly affects the resulting breach size. Indeed, the ship tends to "escape" from the rock and resulting sway, yaw and even roll ship motions limit the damage extent compared to bottom grounding.

Once validated, *FLAGS/MCOL* tool was used to investigate the influence of different structural properties on the breach size. A statistical analysis of the results showed that the most interesting reinforcement strategy consists in increasing the material grade and the outer/side shell thickness. In addition, it was found that the effect of a reinforcement is always less efficient in side grounding than in bottom grounding. Finally, the effect of friction was shown to be of primary importance in bottom grounding while this parameter has almost no effect on the damage extent in side grounding.
Let us conclude by listing some potential developments that would improve the accuracy and reliability of the super-element solver:

1. Small longitudinals attached to outer / inner bottom or side shell have been treated through the smeared thickness approach. Nevertheless, derivation of specific solutions for such components - see *Simonsen* [11] or *Yu et al.* [54] for example - would probably improve the model accuracy.

2. In the current version of FLAGS, the possible reinforcements are limited to thickness, material grade and main scantling of the ship. With the aim of proposing alternative and innovative reinforcement strategies, new super-element formulations could be developed for energy-absorbing structures such as metal foams or other cellular structures that could efficiently dissipate energy - see [55].

[4]CPU time obtained using 8 SMP thread on Intel Xeon CPU E5-2680 V4 at 2.88 GHz

3. Up to now, side grounding scenarios have been treated by giving a surge velocity to the ship. The effect of an initial sway velocity due to an avoidance manoeuvre would also be interesting to investigate. Similarly, the bottom grounding analyses have been performed with the ship having a pure surge velocity. The consideration of the effect of an additional heave/pitch velocity component would deserve to be further studied. This would allow modelling bottom grounding scenarios leading to multiple breaches, as observed in real accidents [30, 56].

4. *FLAGS/MCOL* program could advantageously be coupled with a multi-objective optimisation algorithm in order to investigate alternative ship designs combining the best crashworthiness with an optimised mass. Such work has already been performed for the optimisation of ship-ship collision [57] or in sagging and hogging conditions [58]. A particle swarm optimisation (PSO) solver was coupled with finite element simulations to evaluate the performance of alternative designs. Using the super-element approach is obviously of major interest in such optimisation process as reduced calculation times allow to investigate a wider range of design parameters and grounding scenarios.

Acknowledgments

The research presented in this paper has been carried out under project Flooding Accident Response (FLARE) number 814753, under H2020 programme funded by the European Union. This work has also been partially funded by the French region of Pays de la Loire.

References

1. *IMO. Resolution MSC.421 (98), Amendments to the International Convention for the Safety Of Life At Sea, 1974, as amended, 15 June*
2. *Rodd,* J. L. & *Sikora,* J. P. Double Hull Grounding Experiments. *Proceedings of the Fifth (1995) International Offshore and Polar Engineering Conference* **IV,** 446–456 (1995).
3. *Turgeon,* J. *Analysis of hull damage without fracture in single-bottom transversally framed ships subjected to grounding* tech. rep. (Joint MIT-Industry Program on Tanker Safety, 1995).
4. *Calle,* M. A., *Oshiro,* R. E. & *Alves,* M. Ship collision and grounding: Scaled experiments and numerical analysis. *International Journal of Impact Engineering* **103,** 195–210. doi:10.1016/j.ijimpeng.2017.01.021 (2017).
5. *Chen,* B. Q., *Liu,* B. & *Guedes Soares,* C. Experimental and numerical investigation on the influence of stiffeners on the crushing resistance of web girders in ship grounding. *Marine Structures* **63,** 351–363. doi:10.1016/j.marstruc.2018.10.003 (2019).
6. *Çerik,* B. & *Choung,* J. *On the modelling of strain-rate effects in nonlinear FE analysis of ship collisions* in *International Conference on Ships and Offshore Structures - ICSOS* (Glasgow, UK, 2020).
7. *Echeverry,* S., *Márquez,* L., *Rigo,* P. & *Le Sourne,* H. *Numerical crashworthiness analysis of a spar floating offshore wind turbine impacted by a ship* in *Dev. Collis. Grounding Ships Offshore Struct. - ICCGS 2019* **004** (2020), 85–95. doi:10.1201/9781003002420-11.
8. *Liu,* B. Analysis of structural crashworthiness of double-hull ships based on collision and grounding. *Marine Structures* **3.** doi:10.1016/j.marstruc.2020.102898 (2020).
9. *Prabowo,* A. R., *Cao,* B., *Sohn,* J. M. & *Bae,* D. M. Crashworthiness assessment of thin-walled double bottom tanker: Influences of seabed to structural damage and damage-energy formulae for grounding damage calculations. *Journal of Ocean Engineering and Science.* doi:10.1016/j.joes.2020.03.002 (2020).
10. *Heinvee,* M. *The Rapid Prediction of Grounding Behavior of Double Bottom Tankers. Doctoral thesis* PhD thesis (2016).
11. *Simonsen,* B. C. *Mechanics of Ship Grounding* PhD thesis (1997).
12. *Wang,* G., *Ohtsubo,* H. & *Liu,* D. A simple method for predicting the grounding strength of ships. *Journal of Ship Research* **41,** 241–247 (Sept. 1997).
13. *Zeng,* J., *Hu,* Z. & *Chen,* G. A steady-state plate tearing model for ship grounding over a cone-shaped rock. *Ships and Offshore Structures* **11,** 245–257. doi:10.1080/17445302.2014.985429 (2016).
14. *Hong,* L. & *Amdahl,* J. Rapid assessment of ship grounding over large contact surfaces. *Ships and Offshore Structures* **7,** 5–19. doi:10.1080/17445302.2011.579003 (Mar. 2012).

15. *Puente,* I. J. *Correlation of NSWC grounding tests* tech. rep. (Cambridge, 1995).

16. *Sun,* B., *Hu,* Z. & *Wang,* J. Bottom structural response prediction for ship-powered grounding over rock-type seabed obstructions. *Marine Structures* **54,** 127–143. doi:10.1016/j.marstruc.2017.04.002 (2017).

17. *Pineau,* J., *Le Sourne,* H. & *Soulhi,* Z. *An upper bound solution for the problem of ship bottom plating teared by an elliptic paraboloid shaped rock* in *International Conference on Ships and Offshore Structures* (Glasgow, 2020).

18. *Pineau,* J. P., *Sourne,* H. L. & *Soulhi,* Z. Rapid assessment of ship raking grounding on elliptic paraboloid shaped rock. *Ships and Offshore Structures* **0,** 1–16. doi:10.1080/17445302.2021.1927357 (2021).

19. *Hong,* L. & *Amdahl,* J. Plastic mechanism analysis of the resistance of ship longitudinal girders in grounding and collision. *Ships and Offshore Structures* **3,** 159–171. doi:10.1080/17445300802263849 (2008).

20. *Yu,* Z., *Hu,* Z. & *Wang,* G. Plastic mechanism analysis of structural performances for stiffeners on bottom longitudinal web girders during a shoal grounding accident. *Marine Structures* **40,** 134–158. doi:10.1016/j.marstruc.2014.11.001 (2015).

21. *Alsos,* H. S. & *Amdahl,* J. On the resistance of tanker bottom structures during stranding. *Marine Structures* **20,** 218–237. doi:10.1016/j.marstruc.2007.06.001 (2007).

22. *Nguyen,* T.-H., *Amdahl,* J., *Garrè,* L. & *Leira,* B. A study on dynamic grounding of ships. *Advances in Marine Structures,* 373–380. doi:10.1201/b10771-46 (2011).

23. *Heinvee,* M. & *Tabri,* K. A simplified method to predict grounding damage of double bottom tankers. *Marine Structures* **43,** 22–43. doi:10.1016/j.marstruc.2015.04.002 (2015).

24. *Bulian,* G., *Cardinale,* M., *Dafermos,* G., *Eliopoulou,* E., *Francescutto,* A., *Lindroth,* D., *Luhmann,* H. & *Zaraphonitis,* G. *Considering collision, bottom grounding and side grounding/contact in a common non-zonal framework* in *17th International Ship Stability Workshop* (Helsinki, 2019), 10–12.

25. *Bulian,* G., *Cardinale,* M., *Dafermos,* G., *Lindroth,* D., *Ruponen,* P. & *Zaraphonitis,* G. Probabilistic assessment of damaged survivability of passenger ships in case of grounding or contact. *Ocean Engineering* **218,** 107396. doi:10.1016/j.oceaneng.2020.107396 (2020).

26. *Taimuri,* G., *Kim,* S., *Mikkola,* T. & *Hirdaris,* S. A Two-way coupled FSI model for the rapid evaluation of accidental loads following ship hard grounding events. *J. Fluids Struct.,* 103589. doi:10.1016/j.jfluidstructs.2022.103589. https://doi.org/10.1016/j.jfluidstructs.2022.103589 (2022).

27. *Yu,* Z., *Hu,* Z., *Wang,* G. & *Liu,* K. *An Analysis of Structural Performances for Bottom Longitudinal Girder and Attached Stiffeners During Shoal Grounding Accident* 2013.

28. *Heinvee,* M., *Tabri,* K., *Kõrgesaar,* M. & *Urbel,* A. Influence of longitudinal and transverse bulkheads on ship grounding resistance and damage size. *Proceedings of International Conference on Collision and Grounding of Ships and Offshore Structures,* 99–109 (2016).

29. *Le Sourne,* H., *Donner* R.and Besnier, F. & *Ferry,* M. External Dynamics of Ship-Submarine Collision. *2nd International Conference on Collision and Grounding of Ships (ICGS),* 137–144 (2001).

30. *Le Sourne,* H., *Pineau,* J., *Umunnakwe,* C., *Wesoly,* T. & *Dorival,* O. *On the influence of buoyancy forces, failure strain and friction coefficient on the damage extent of a grounded ship* in *Marine Structures - MARSTRUCT* (Trondheim, 2021).

31. *Lützen,* M. *Ship Collision Damage* PhD thesis (Technical university of Denmark, 2001). doi:10.1111/j.1365-2958.2006.05502.x.

32. *Le Sourne,* H., *Besnard,* N., *Cheylan,* C. & *Buannic,* N. A Ship Collision Analysis Program Based on Upper Bound Solutions and Coupled with a Large Rotational Ship Movement Analysis Tool. *Journal of Applied Mathematics* **2012,** 1–27. doi:10.1155/2012/375686 (2012).

33. *Le Sourne,* H., *Pineau,* J., *Looten,* T., *Conti,* F., *Kaydihan,* L., *Bae,* E., *Vassalos,* D., *Kujala,* P. & *Hirdaris,* S. *A comparison of crashworthiness methods for the assessment of ship damage extents* in *1st International Conference on the Stability and Safety of Ships and Ocean Vehicles* (Glasgow, 2021).

34. *Jones,* N. *Structural Impact* doi:DOI:10.1017/CBO9780511624285 (Cambridge University Press, Cambridge, 1990).

35. *Pedersen,* P. T. & *Li,* Y. On the global ship hull bending energy in ship collisions. *Marine Structures* **22,** 2–11. doi:10.1016/j.marstruc.2008.06.005 (2009).

36. *Paik,* J. Cutting of a longitudinally stiffened plate by a wedge. *Journal of Ship Research* **38,** 340–348 (1994).

37. *Little,* P. *A study of the wedge cutting force through transversely stiffened plates: an application to ship grounding resistance* tech. rep. (1994).

38. *Pippenger,* D. T. *Coupled vertical and horizontal resistance of hull girder in grounding accidents* tech. rep. (1995).

39. *Bracco,* M. A Study on the Wedge Cutting Force through Longitudinally Stiffened Plates An Application to Grounding Resistance of Single and Double Hull Ships (1994).

40. *Liu,* Y., *Hu,* Z. & *Amdahl,* J. *Investigation on smeared thickness method for plating stiffeners on prediction of grounding character of double bottom tanker over obstacles with large contact surface* in *Proceedings of the International Conference on Offshore Mechanics and Arctic Engineering - OMAE* **2** (2012), 115–122. doi:10.1115/OMAE2012-83238.

41. *Ferry,* M., *Le Sourne,* H. & *Besnier,* F. MCOL-theoretical manual. *Principia Marine, Nantes* (2002).

42. *Marine Principia. MCOL-User's Manual* tech. rep. (2002).

43. *Kim,* S.-j. *et al.* Comparison of numerical approaches for structural response analysis of passenger ships in collisions and groundings. *Mar. Struct.* **81,** 1–32. doi:10.1016/j.marstruc.2021.103125 (2021).

44. *Luhmann,* H. *Integrated flooding and standard for stability and crises management* tech. rep. October (2009), 202.

45. *Paik,* J. K. & *Thayamballi,* A. K. *Ultimate limit state design of steel plated structures* English. Chichster, England; Hoboken, NJ, 2003.

46. *Hallquist,* J. *LS-DYNA Theory Manual* tech. rep. (2006).

47. *Scharrer,* M. & *Zhang,* L. *Kollisions-berechnungen in schiffbaulichen entwurfssystemen (collision calculation in naval design systems)* tech. rep. (Germanischer Lloyd, 2002).

48. *Conti,* F., *Le Sourne,* H., *Vassalos,* D., *Kujala,* P., *Lindroth,* D., *Kim,* S. J. & *Hirdaris,* S. A comparative method for scaling SOLAS collision damage distributions based on ship crashworthiness–application to probabilistic damage stability analysis of a passenger ship. *Ships and Offshore Structures* **0,** 1–17. doi:10.1080/17445302.2021.1932023 (2021).

49. *Youssef,* S. A. M. & *Paik,* J. K. Hazard identification and scenario selection of ship grounding accidents. *Ocean Engineering* **153,** 242–255. doi:10.1016/j.oceaneng.2018.01.110 (2018).

50. *Conti,* F. *FLARE D3.4 - Annex C : Comparative method for derivation of bottom grounding damage distributions taking into account ship crashworthiness* tech. rep. (2021).

51. *DNV GL. Evaluation of risk from raking damages due to grounding, Final report.* tech. rep. (2015).

52. *Conti,* F. *Comparative Method for the Derivation of Side Grounding Damage Distributions Taking Into Account Ship Crashworthiness* tech. rep. (2022).

53. *Le Sourne,* H. *A ship Collision Analysis Program Based on Super-element Method Coupled with Large Rotational Ship Movement Analysis* in *4th International Conference on Collision and Grounding of Ships* (Hamburg, 2007), 131–138.

54. *Yu,* Z., *Hu,* Z. & *Wang,* G. Plastic mechanism analysis of structural performances for stiffeners on bottom plate during shoal grounding accident. *Analysis and Design of Marine Structures,* 219–229. doi:10.1201/b15120-30 (2013).

55. *Kremer,* K. *Metal Foams for Improved Crash Energy Absorption in Passenger Equipment* tech. rep. September (Center for Manufacturing and Advanced Materials, 2004).

56. *Papanikolaou,* A. D., *Bulian,* G. & *Mains,* C. *GOALDS – Goal Based Damaged Stability : Collision and Grounding Damages* in *12th International Ship Stability Workshop* (2009), 37–44.

57. *Ehlers,* S. A procedure to optimize ship side structures for crashworthiness. *Proceedings of the Institution of Mechanical Engineers Part M: Journal of Engineering for the Maritime Environment* **224,** 1–11. doi:10.1243/14750902JEME179 (2010).

58. *Raikunen,* J., *Avi,* E., *Remes,* H., *Romanoff,* J., *Lillemäe-Avi,* I. & *Niemelä,* A. Optimisation of passenger ship structures in concept design stage. *Ships Offshore Struct.* **14,** 320–334. doi:10.1080/17445302.2019.1590947 (2019).

A FLAGS GUI

The *FLAGS/MCOL* graphical interface depicted in Figure 21 is constituted of three different areas. The first one (orange box) allows to select the project, create a video, change the camera angle etc... In the second area (blue rectangle), the impacted Super-Elements are highlighted in different colours depending on their state (non-impacted, impacted, ruptured, deleted) and the position (translation and rotation) of the ship is updated at each time step. Finally, in the third area (red box), the time evolution of resisting forces, dissipated energies, ship displacements, velocities and other quantities available in the result file may be visualised.

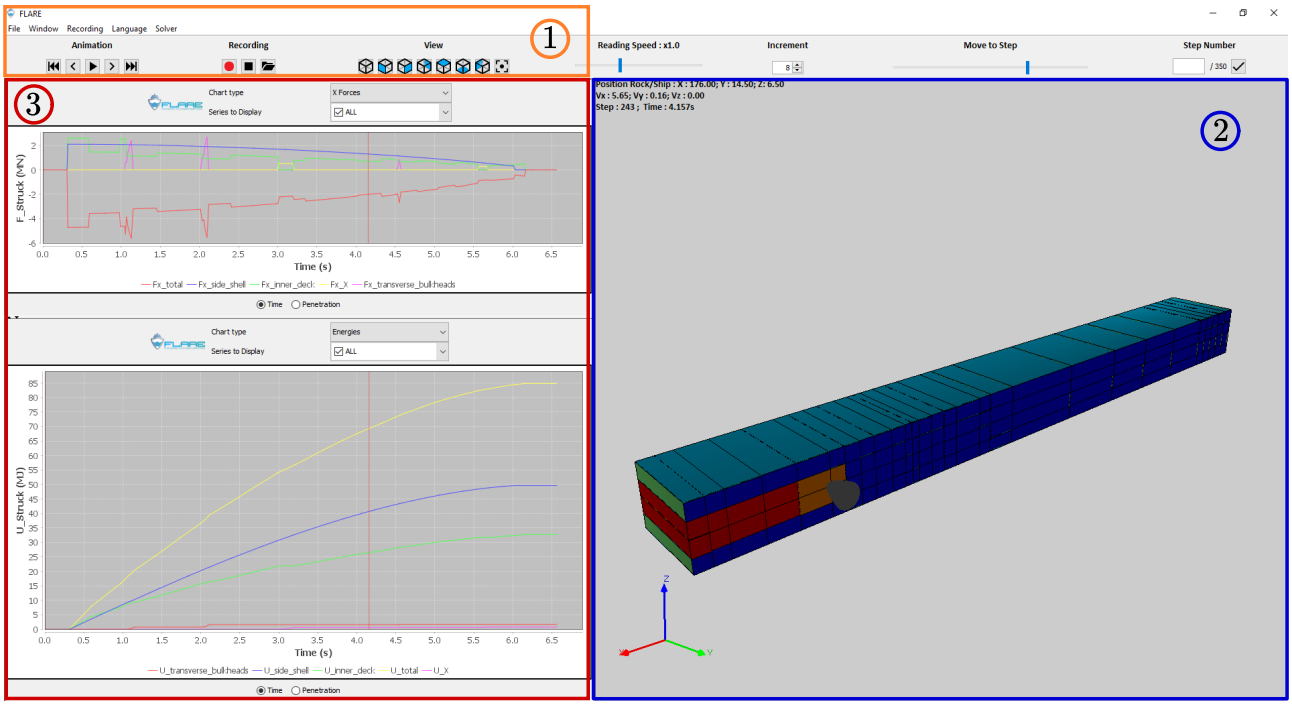

Figure 21: *FLAGS/MCOL* Graphical User Interface

B Theoretical reduction factor

This appendix is dedicated to the derivation of the Upper and Lower bound of the breach reduction factor λ in side grounding.

The simplified damage length in side grounding is given by :

$$L(\tau) = -\frac{F_L M_T}{F_T M_L} H + v_{x0} \sqrt{\frac{2HM_T}{\tau F_T}} \tag{25}$$

Resulting theoretical reduction factor λ thus writes:

$$\lambda = \frac{L(\tau) - L(1)}{L(1)} \tag{26}$$

Or in its extended forms :

$$\lambda = v_{L0} \sqrt{\frac{2HM_T}{F_T}} \frac{\frac{1}{\sqrt{\tau}} - 1}{-\frac{F_L M_T}{F_T M_L} H + v_{L0} \sqrt{\frac{2HM_T}{F_T}}} \tag{27}$$

Let β and α defined as :

$$\beta = v_{L0} \sqrt{\frac{2HM_T}{F_T}} \tag{28}$$

$$\alpha = \frac{F_L M_T}{F_T M_L} H \tag{29}$$

In the case of reinforcement $\frac{1}{\sqrt{\tau}} - 1 < 0$ and since $-\alpha < 0$, one can show :

$$\lambda = \frac{\beta}{\beta - \alpha}\left(\frac{1}{\sqrt{\tau}} - 1\right) \leq \frac{\beta}{\beta}\left(\frac{1}{\sqrt{\tau}} - 1\right) = \frac{1}{\sqrt{\tau}} - 1 \tag{30}$$

Therefore $\frac{1}{\sqrt{\tau}} - 1$ constitute an Upper-bound for λ.

Dealing with the Lower-bound is a bit more complex. However by noticing that β corresponds to the distance travelled by the ship without any deceleration, and $\beta - \alpha$ correspond to the distance travelled by the ship considering the effect of the deceleration. Therefore, $\beta/(\beta - \alpha)$ may be rewritten as :

$$R = \frac{\beta}{\beta - \alpha} = \frac{v_{L0}t_0}{-F_L/M_L t_0^2/2 + v_{L0}t_0} \tag{31}$$

For the floodstand ship B, the ship inertia M_L is 34 325 *tons*, the average resisting force F_L is 2.5 *MN*, therefore the expected ratio R remains lower than 1.2 - see Figure 22. The lower bound is then :

$$1.2\left(\frac{1}{\sqrt{\tau}} - 1\right) \leq \lambda \tag{32}$$

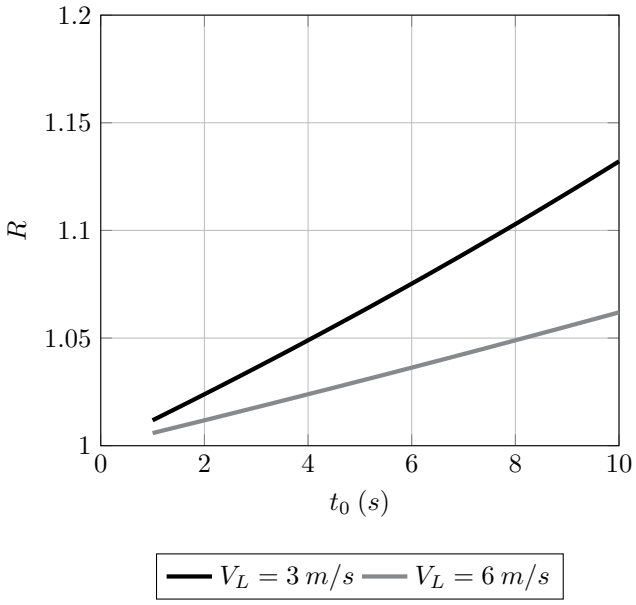

Figure 22: Lower bound for λ factor - Side grounding

Using Eq. 30 and Eq. 32 we finally obtain :

$$1.2\left(\frac{1}{\sqrt{\tau}} - 1\right) \leq \lambda \leq \frac{1}{\sqrt{\tau}} - 1 \tag{33}$$

C Effect of a reinforcement

Assuming one wishes to decrease the damage length in both bottom and side grounding by $X\%$, then using Eq. 18 and Eq. 33 one can have :

$$\frac{1}{\tau_{Bottom}} - 1 = k\left(\frac{1}{\sqrt{\tau_{Side}}} - 1\right) \tag{34}$$

Where k lies between 1 and 1.2, then τ_{Side} may be expressed as :

$$\tau_{Side} = k^2 \frac{\tau_{Bottom}^2}{1 + \tau_{Bottom}(k-1)} \tag{35}$$

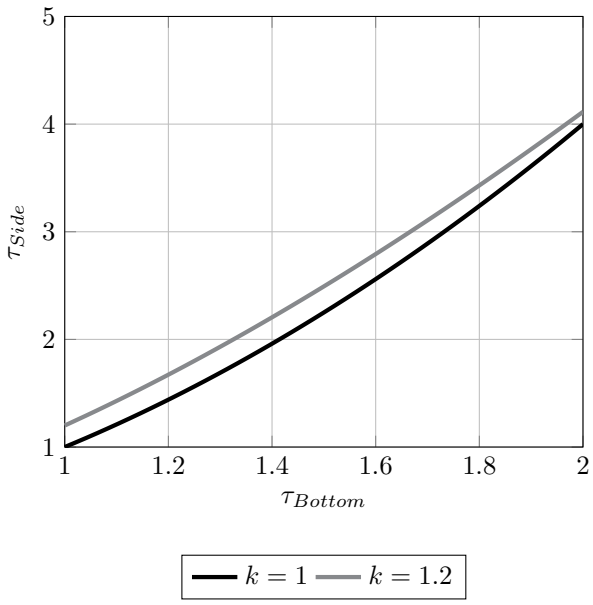

Figure 23: τ_{Side} as a function of τ_{Bottom}

Using Eq. 35 or Figure 23, it can be concluded that in order to reduce by $X\%$ the damage length in both bottom and side grounding the reinforcement to be applied in side grounding must $\tau_{Side}/\tau_{Bottom} \approx \tau_{Bottom}$ more important than the one to be applied in bottom grounding.

D EMSA data

Figure 24 below shows the damage domains obtained from the analysis of real grounding events within the framework of EMSA3 European research project [51] as well as damage extents post-processed from FLAGS/MCOL simulations based on parametric values listed in Table 11.

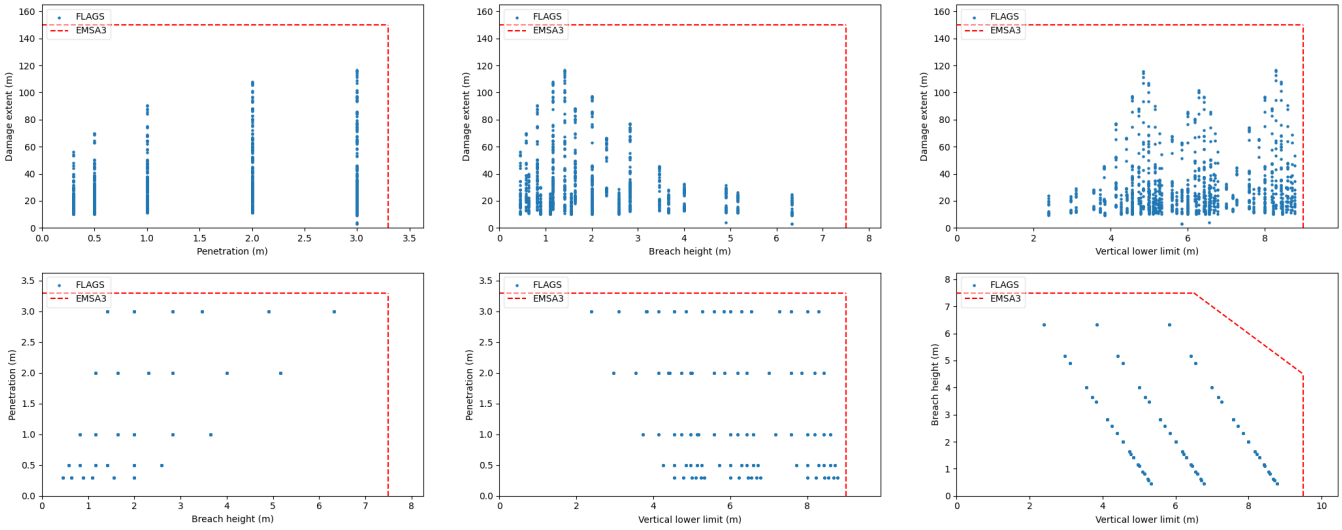

Figure 24: Comparison of EMSA3 damage domains with FLAGS/MCOL results